SLAC–PUB–5222
October 1990
(A)

A DISPERSION-FREE TRAJECTORY CORRECTION TECHNIQUE FOR LINEAR COLLIDERS*

T. O. RAUBENHEIMER and R. D. RUTH

Stanford Linear Accelerator Center, Stanford University, Stanford, CA 94309 USA

Abstract

In this paper, we describe a new trajectory correction technique for high energy linear accelerators. Current correction techniques force the beam trajectory to follow misalignments of the Beam Position Monitors (BPMs). Since the particle bunch has a finite energy spread and particles with different energies are deflected differently, this causes "chromatic" dilution of the transverse beam emittance. The algorithm which we describe in this paper reduces the chromatic dilution by minimizing the energy dependence of the trajectory. To test the method we compare the effectiveness of our algorithm with a standard correction technique in simulations of the Stanford Linear Collider (SLC) linear accelerator and a design linac for a Next Linear Collider (NLC). While the simulations do not indicate that chromatic dilutions are a serious problem in the SLC linac, they would be debilitating in a future linear collider because of the very small beam sizes required to achieve the necessary luminosity. For example, in simulations of the NLC we have found that with typical alignment tolerances the beam size increased substantially after correcting the trajectory with a standard correction algorithm. In contrast, after correcting with our technique, the dilution was negligible. We feel that this technique will prove essential for future linear colliders.

Submitted to Nuclear Instruments and Methods

*Work supported by the Department of Energy, contract DE–AC03–76SF00515.

1. Introduction

In a linear collider there are many effects which dilute the beam emittance; a measure of the phase-space volume occupied by the beam. The dilution then causes a reduction in the collider's luminosity. In this paper, we discuss a new trajectory correction technique for linear accelerators which reduces the "chromatic" emittance dilution.

The chromatic emittance dilution results from "dispersive errors." Dispersive errors occur when the beam trajectory is deflected since the deflections differ for particles with different energies. Because the particle beam has a finite energy spread, these dispersive errors cause a dilution of the transverse emittance; we refer to this dilution as a chromatic dilution. The chromatic emittance dilution tends to scale with the transverse alignment tolerances in the linac relative to the beam size. Since, to achieve the necessary luminosity, the beam sizes in most future linear collider designs are very small, the chromatic dilution, if uncorrected, would specify very tight alignment tolerances.

The trajectory in a linac needs to be corrected because misalignments and stray fields deflect the beam. In addition to aperture limitations, the orbit offsets lead to wakefields and dispersive errors which dilute the transverse emittance. To reduce these effects, the trajectory is corrected with additional dipole correctors. Usually, the correction algorithms attempt to zero the Beam Position Monitors (BPMs) which measure the trajectory in the linac. For example, in the Stanford Linear Collider (SLC) linac, a "one-to-one" algorithm is used to implement the correction. Here, a single dipole corrector is used to zero a single (downstream) BPM. Using this algorithm, each of the matched BPMs can be zeroed within the limitations of the corrector strength and the BPM precision, *i.e.*, the intrinsic noise in the BPM measurements.

The problem with this technique is that the BPMs are typically misaligned, both electronically and mechanically. Thus, the corrected trajectory is kicked from side to side, following the BPM misalignments. In such a case, the chromatic dilution tends to grow with the square root of the number of BPMs [3]. For example, it is estimated in ref. [3] that 30 μm BPM misalignments in the NLC [2], a future linear collider design, would cause the vertical emittance to double when using the one-to-one correction technique. To reduce this dilution to 25%, we would need to align the multikilometer linac to roughly 10 μm. This is about one order of magnitude better alignment than can be achieved with techniques now in practice

To avoid this situation, we need to either find and correct the BPM misalignments or develop an algorithm which does not depend upon the BPM alignment errors. A method of using the beam to find the quadrupole and BPM misalignments has been developed for the SLC linac [4,5]. The method uses trajectory information from two or more different focusing configurations to solve for the individual misalignments; the focusing configuration of the machine is varied by tuning the quadrupole magnets which focus the beam throughout the linac. While this method has been used very successfully to find most of the large alignment errors, in the SLC, it is limited to an accuracy of roughly 100 μm [4].

In this paper, we discuss an algorithm which is less dependent on the BPM misalignment errors than the one-to-one algorithm. Our approach is similar to that of Refs. [4] and [5], in that we use information from two different focusing configurations. Specifically, we measure two trajectories where we change the focusing structure between measurements. By subtracting these two trajectories, the resulting difference orbit is *independent* of the BPM alignment errors. In theory, the quadrupole misalignments could now be found. Unfortunately, the

difference orbit still has errors due to the finite BPM precision and additional unknown deflections. Rather than trying to solve for the ***individual*** misalignments, we simply correct the trajectory to minimize the difference orbit; this will then minimize the dispersive error.

In the next section, we discuss the basic theory and some aspects of the implementation. In sec. 3, we perform a detailed analysis of errors affecting the correction technique. In sec. 4, we present results from simulating the correction technique on the SLC linac and a preliminary design for the NLC linac, comparing with results found using the one-to-one algorithm. Next, we compare with another method of controlling the chromatic dilution. Finally, in sec. 6 we discuss the effect of alignment tolerances on our algorithms.

2. Theory

2.1 Beam transport

A particle beam consists of particles distributed in a six-dimensional phase-space: $(x, p_x,\ y, p_y,\ \delta, l)$ where x and y are the transverse coordinates, p_x and p_y are the transverse momenta, and δ and l are the relative energy deviation and longitudinal position. To constrain the transverse size of the beam, it is transported through a focusing structure, which, in the case of high-energy beams, is usually constructed from an array of quadrupole magnets. The envelope of the transverse beam distribution is defined by this focusing structure and the initial conditions. As the beam propagates, the particles execute transverse betatron oscillations about the beam centroid within this envelope.

Since the quadrupole magnets provide linear focusing, the particle trajectories can be described by a transport matrix, relating a particle's position to its initial

conditions and the deflections due to additional dipole fields. Likewise, the trajectory of the beam centroid can be expressed in the same manner; the centroid follows the trajectory of a fictitious central particle that defines the *central* trajectory of the bunch. Assuming that the horizontal and vertical planes are uncoupled, the particle position can be expressed as

$$x(s) = x_0 R_{11}(s_0, s) + x'_0 R_{12}(s_0, s) + \sum_i \theta_i R_{12}(s_i, s) \quad , \tag{1}$$

where x_0 and x'_0 are the initial conditions and θ_i are the deflections due to additional dipole fields. The coefficient R_{11} and R_{12} are matrix elements relating positions and deflections at one location to a position at another location; these only depend upon the focusing structure of the machine.

2.2. Dispersive errors and chromatic dilutions

In this paper, we differentiate between the "dispersive errors" and the chromatic dilution of the bunch. Specifically, we use the terms "dispersive error" or "dispersion" to describe the variation of the *central* trajectory with energy; it is a single particle effect. We define the "dispersive error" of a particle with an energy deviation as the difference between its trajectory and the trajectory of a particle with the design energy $E(s)$.

Dispersive errors arise because particles with different energies are deflected differently; for ultrarelativistic particles, the deflections scale inversely with the beam energy. Thus, for a particle with energy $(1 + \delta(s))E(s)$, the dispersive error is

$$\Delta x(s) = \sum_i \theta_i \left[R_{12}(s_i, s) - (1 - \delta_i) R_{12}(\delta; s_i, s) \right] \quad , \tag{2}$$

where we have set the initial conditions x_0 and x_0' to zero. The parameter θ_i is the deflection at longitudinal position s_i and includes kicks from both correctors and errors, δ_i is the relative energy deviation from the design energy, $E_0(s)$: $\delta_i \equiv (E(s_i) - E_0(s_i))/E(s_i)$, and the matrix element $R_{12}(s_i, s)$ transforms a deflection at s_i to a transverse position at s; the coefficient $R_{12}(\delta)$ is the R_{12} matrix element for a particle with energy deviation $\delta(s)$. Finally, we should mention that the dispersion is a nonlinear function of δ; this is seen in the $R_{12}(\delta)$ matrix elements. This nonlinearity will be important for the discussion of errors in sec. 3.

As has been mentioned, a particle beam consists of particles distributed a six-dimensional phase-space. Chromatic dilution of the transverse phase-spaces occurs for two reasons: first, the dispersive errors will cause each constant energy slice of the beam distribution to have a different centroid; they will follow different central trajectories. Second, the beam envelopes of the constant energy slices, *i.e.*, the second-order moments of the slices, will differ since particles with different energy experience different focusing.

In this paper, we discuss correcting only the first contribution to the chromatic dilution. If the focusing structure of the accelerator is properly adjusted the second effect will typically be small. For example, in the SLC and NLC linacs this effect leads to less than 0.1% emittance dilution. Of course, when the linac is not properly "matched," *i.e.*, the focusing structure of the linac is not set correctly, this second effect can become large. Regardless, matching the linac is a separate issue and we will not treat it in this report.

2.3. Trajectory correction

To reduce the chromatic emittance dilution, we correct the energy-dependence of the central trajectory. To do this, we vary the *effective* beam energy and then

correct the difference of the resulting orbit and the original trajectory. In a linac, there are two methods of changing the effective energy: changing the beam energy or, equivalently, changing the magnet strengths; increasing all of the magnets by 1% has the same effect on the transverse optics as decreasing the local beam energy by 1%.

To correct the difference orbit resulting from changing the effective beam energy, we need to measure the beam trajectories. If we consider only transverse quadrupole misalignments and dipole correctors, the ith BPM will measure

$$m_i = \xi_i(t_1) - b_i + x_0 R_{11}(s_0, s_i) + x_0' R_{12}(s_0, s_i) + \sum_j^{N_c} \theta_j R_{12}(s_j, s_i) + \sum_{j=1}^{N_q} d_j \mathcal{R}_{ij} \quad , \tag{3}$$

where ξ is a stochastic variable representing the BPM precision error, θ is the deflection of the dipole correctors, and, b and d are the BPM and quadrupole misalignments relative to the linac centerline. The coefficients $R_{11}(s_0, s_i)$ and $R_{12}(s_0, s_i)$ are two elements of the transport matrix which relate the initial values x_0 and x_0' to a position offset at the ith BPM. Likewise, $R_{12}(s_j, s_i)$ relates the deflection due to the jth corrector to a position at the ith BPM. Finally, we have a sum over the quadrupole magnets where $\mathcal{R}_{ij}$ relates d_j, the misalignment of the jth quadrupole, to a position offset at the ith monitor. Specifically,

$$\mathcal{R}_{ij} = R_{11}(s_i, s_j)(1 - \cos\sqrt{K}L) + R_{12}(s_i, s_j)\sqrt{K}\sin\sqrt{K}L \quad , \tag{4}$$

where the jth quadrupole has normalized strength $K = (e/\beta\gamma mc^2)dB_y/dx$ and length L, and the quadrupole magnet ends at s_j. Obviously, $\mathcal{R}_{ij}$ is zero if $s_i < s_j$.

In a similar manner, we can calculate the measured trajectory after the effective beam energy is changed by $\delta(s) \equiv \Delta E(s)/E(s)$. The difference orbit that we will

correct is found by subtracting this new trajectory from the original measured trajectory:

$$\Delta m_i = \left(\xi_i(t_1) - \xi_i(t_2)\right) + x_0\overline{R_{11}}(\delta;\, s_0,\, s_i) \,+\, x_0'\overline{R_{12}}(\delta;\, s_0,\, s_i) + \sum_{j=1}^{N_c} \theta_j \overline{R_{12}}(\delta; s_j, s_i) + \sum_{j=1}^{N_q} d_j \overline{\mathcal{R}_{ij}}(\delta) \quad . \tag{5}$$

Here, $\overline{R}(\delta) \equiv R - R(\delta)$ and $R(\delta)$ is the coefficient R calculated for the modified optics due to the change in energy. It is important to notice that the difference orbit is independent of the BPM misalignments. We should also note that we have not included additional unknown errors such as RF deflections or magnetic strength errors; these and other errors will be discussed in sec. 3.

In principle, using $(N_q + 2)$ BPMs, we could solve for the quadrupole misalignments and the initial conditions exactly, ***provided*** that the BPM precision errors and any additional deflections are negligible. In such a case, we could fix the injection and the quadrupole errors; the trajectory would then follow the linac centerline and the dispersive error would be zero. Obviously, this is not realistic. When the additional errors are included, the difference orbit is not a function of **just** (N_q+2) unknowns. Thus, we cannot calculate the ***individual*** quadrupole misalignments and the initial conditions exactly. The error in each calculated value will increase with the number of misalignments being estimated since each calculation depends upon the accuracy of the preceding calculations. Of course, while the error of each individual calculation may be large, the global solution could be used to reduce the difference orbit to the level of the BPM precision errors. Unfortunately, after correcting the difference orbit, and thereby the dispersive error, we would find that the trajectory would diverge from the linac centerline. This occurs since the difference orbit is not referenced to the linac centerline.

It is evident that we need to include some information about the real trajectory while correcting the difference orbit. We have found that the best approach is to perform a least squares solution for the unknowns using both the original trajectory and the difference orbit with the appropriate weighting. Thus, we solve for the dipole corrector strengths which minimize the sum

$$\sum_{j=1}^{N_q} \frac{(m_j + X_j)^2}{\sigma_{\rm prec}^2 + \sigma_{\rm BPM}^2} + \frac{(\Delta m_j + \Delta X_j)^2}{2\sigma_{\rm prec}^2} \quad . \tag{6}$$

Here, $\sigma_{\rm prec}$ is the RMS of the BPM precision errors and $\sigma_{\rm BPM}$ is the RMS of the BPM misalignments relative to the linac centerline. In addition, X_j is the predicted trajectory at the jth BPM as a function of the dipole corrector strengths and ΔX_j is the predicted difference orbit. We will subsequently refer to this algorithm as Dispersion-Free (DF) correction.

It is important to note that with this algorithm, the correction of the dispersive error, *i.e.*, the difference orbit, is independent (approximately) of the magnitude of the BPM misalignments. Instead, the correction depends upon the BPM precision and the accuracy with which the measured difference orbit reflects the dispersive error.

2.4. Emittance dilution

To compare the results of the correction algorithms, we need to calculate the emittance increase due to the dispersion. We will discuss the actual emittance at the end of the linac, *i.e.*, the area the beam fills in phase-space. Of course, the beam will continue to filament as it is transported to its final destination. Furthermore, in a linear collider, one is interested in the overlap of the two colliding beams. Thus, the *effective* emittance increase may differ from the actual increase. Unfortunately,

this effective increase is dependent upon the downstream optics, etc., and thus we only consider the actual phase-space increase.

The transverse emittance of a particle bunch is given by [1]

$$\epsilon = \sqrt{\langle x^2 \rangle \langle x'^2 \rangle - \langle x x' \rangle^2} \quad , \tag{7}$$

where the angle brackets denote an average over the particle distribution and the coordinates x and x' are referred to the beam centroid. Assuming that the dispersive errors are a linear function of the energy difference (valid for small $\Delta E/E$), the emittance is

$$\epsilon = \epsilon_0 \sqrt{1 + \mathcal{F}_\pm / \epsilon_0} \quad . \tag{8}$$

Here, ϵ_0 is the unperturbed emittance and it is multiplied by a magnification factor. The function $\mathcal{F}$ is

$$\mathcal{F}_\pm = \beta \Delta x_{\sigma\pm}^2 + 2\alpha \Delta x_{\sigma\pm} \Delta x'_{\sigma\pm} + \gamma \Delta x'^2_{\sigma\pm} \tag{9}$$

where β, α, and γ are the lattice parameters for the design energy [6]. In particular, β, α, and γ are proportional to the second moments of the unperturbed beam distribution: $\langle x^2(s) \rangle = \epsilon_0 \beta(s)$, $\langle x x'(s) \rangle = -\epsilon_0 \alpha(s)$, and $\langle x'^2(s) \rangle = \epsilon_0 \gamma(s)$.

The function $\mathcal{F}$ is similar in form to the "curly H" function introduced to calculate the emittance in storage rings [7]. It is a function of the difference orbit Δx_σ, which is the difference between the trajectory of a particle with the design energy and a particle whose energy differs from the design by the RMS energy spread:

$$\Delta x_{\sigma\pm} \equiv x(E_0 \pm \sigma_\epsilon) - x(E_0) \quad . \tag{10}$$

Here, $\sigma_\epsilon(s)$ is the RMS relative energy spread and x is the beam trajectory; note that both $\sigma_\epsilon(s)$ and $E_0(s)$ are functions of position s. This difference orbit is a measure of the chromatic dilution; we will use it to estimate the effect of errors in the correction algorithm in the next section.

Now, we need to allow for the nonlinearity of the dispersion. Notice that, if the errors were linear functions of $\Delta E/E$, $\Delta x_{\sigma+}$ would equal the negative of $\Delta x_{\sigma-}$ and $\mathcal{F}_+$ would equal $\mathcal{F}_-$. Since the dispersion is not linear, we compute the emittance as an average, using both the $\Delta x_{\sigma+}$ and $\Delta x_{\sigma-}$ difference orbits:

$$\epsilon \approx \frac{\epsilon_0}{2}\left[\sqrt{1+\frac{\mathcal{F}_+}{\epsilon_0}}+\sqrt{1+\frac{\mathcal{F}_-}{\epsilon_0}}\right] \quad . \tag{11}$$

Here, we are approximating the emittance with half of the beam ellipse extended by $\pm\Delta x_{\sigma+}$ and half of the ellipse extended by $\pm\Delta x_{\sigma-}$. Usually, this definition of the magnification factor will tend to underestimate the core emittance since we are approximating a curve with two straight lines. Of course, it is possible that eq. (11) will overestimate the magnification. This will occur if the inner core of the beam is much more densely packed than the outer envelope; in this case, the one-sigma-point cannot be used to accurately reflect the density of the beam. Regardless, we have generally found good agreement between eq. (11) and actual beam emittance.

Finally, we discuss the basic scaling of the emittance with the magnitude of the misalignments. The difference orbit Δx_σ is roughly proportional to the magnitude of the misalignments causing the dispersive errors. Thus, when the dispersion is large $\Delta x_\sigma \gg \sqrt{\beta\epsilon}$, the emittance increase is also roughly proportional to the magnitude of the misalignments. In contrast, when the dispersion is small, the increase is proportional to the square of the misalignment magnitude.

3. Error Analysis

In this section, we analyze the effect of various errors on the performance of the DF correction algorithm. In a linac, there are many additional errors that were not included in the initial formulation of the DF algorithm. Thus, to understand the utility of the algorithm, we have to determine its sensitivity to these additional errors.

The DF algorithm corrects the dispersive error by correcting a measured difference orbit which is created by changing the effective beam energy. Thus, the algorithm relies upon the *resemblance* between this measured difference orbit and the actual dispersive error. We can divide any errors into two catagories: errors which cause the measured difference orbit to differ from the actual difference orbit (measurement errors) and errors which cause the difference orbit to differ from the dispersive error of a particle within the beam.

Errors in neither category will not degrade the correction of the chromatic dilution and thus can be ignored. This is an important aspect of the algorithm. The algorithm does not attempt to extract specific information from noisy data; it minimizes a *measured* quantity. Thus, if errors reduce the convergence of the minimization, one can simply iterate the correction procedure. Examples of such errors are BPM and corrector calibration errors, absolute beam energy errors, and errors in the transport coefficients R_{12} used to calculate the corrections. These errors will only slow the convergence of the algorithms. Rather than requiring one iteration, perhaps two or even three iterations will be required to achieve a good solution.

In contrast, errors in the first two catagories will cause the algorithm to converge to an incorrect solution. BPM precision and beam jitter errors are examples of

errors from the first category. Magnet scaling errors, RF deflections, and effects due to the nonlinearity of the dispersion are examples of errors in the second category. We will first discuss effects due to the nonlinearity of the dispersive error and then we will discuss each of the other effects in turn. We proceed in this order since the nonlinearity is important for determining the full effect of the BPM precision and beam jitter errors.

3.1. Nonlinearity

The goal of our correction algorithm is to improve the transverse emittance dilution due to the dispersive error; we want to correct the dispersive error arising from the energy variation within the particle bunch. As mentioned in sec. 2.2, the dispersion is a nonlinear function of the energy deviation. Thus, ideally, we would like to measure the difference orbit by making an effective energy change comparable to the bunch energy spread. Unfortunately, this tends to be small, the order of 1% or less, and we will see that a small effective energy change can lead to large errors in the corrected solution. Therefore, we need to determine the effect of correcting a difference orbit created by an energy change that is substantially different from the beam energy spread.

In eq. (2), we expressed the difference orbit in a form that implicitly includes the exact dependence on the energy deviation. Here, we need an expression for the difference orbit that explicitly displays the dependence. The equation of motion for a particle in a transport line can be written [1]

$$x''(s) + (1-\delta)K(s)x(s) = (1-\delta)G(s) \quad , \tag{12}$$

where $K(s)$ is the normalized quadrupole strength and $G(s) = 1/\rho$ is the inverse of the local bending radius due to dipole deflections. Note that for simplicity we have not included effects due to the acceleration in eq. (12).

We can use eq. (12) to find the equation for the difference orbit $\Delta x_\delta = x_0 - x_\delta$ due to an energy change of δ.

$$\Delta x_\delta'' + K\Delta x_\delta = \delta\big(G - Kx_0 + K\Delta x_\delta\big) \quad , \tag{13}$$

where x_0 is the on-energy trajectory and we have used the subscript δ to refer to the magnitude of the energy change which created the difference orbit. We solve this equation perturbatively, treating all elements as infinitely thin in length, *i.e.*, delta-functions in s. To second order, this yields

$$\Delta x_\delta(s) = \Delta x_\delta^{(1)}(s) + \sum_i \delta_i (KL)_i \Delta x_\delta^{(1)}(s_i) R_{12}(s, s_i) \quad , \tag{14}$$

where the first order term is

$$\Delta x_\delta^{(1)}(s) = \sum_i \delta_i \Big((GL)_i - (x_i - d_i)(KL) \Big) R_{12}(s, s_i) \quad . \tag{15}$$

Here, x_i and d_i are the on-energy trajectory and misalignment at the ith quadrupole, and GL and KL are the integrated deflection due to a dipole field and the integrated quadrupole strength, respectively.

Equation (14) illustrates a potential problem of using an energy change δ that is substantially larger than the beam energy spread $\sigma(s)$. If δ is relatively large, it is possible to correct the resulting difference orbit Δx_δ to a small value while having a large first order contribution $\Delta x_\delta^{(1)}$; the second order contribution can be used to cancel the first order term. Unfortunately, this cancellation does not work

within the beam since the beam energy spread is small. Thus, one can correct Δx_δ while actually increasing the chromatic dilution of the beam. In the subsequent sections, we will use eqs. (14) and (15) to determine the effect of errors on the DF correction algorithm.

3.2. BPM precision

The BPM precision errors will limit the accuracy with which we can correct the difference orbit. Assuming that the BPMs have random precision errors with a RMS of $\sigma_{\rm prec}$, the measured difference orbit will differ from the actual difference orbit by an RMS error of $\sqrt{2}\sigma_{\rm prec}$. We can estimate the residual dispersive error, after correcting this measured difference orbit, by considering a simplified example where one zeros the measured difference orbit at each of the BPMs. After correction, the actual difference orbit Δx_δ would be equal to the negative of the BPM precision errors.

Given this residual difference orbit Δx_δ, we want to solve for the difference orbit Δx_σ created by an energy change of $\sigma(s)$, where σ is the RMS energy spread. This will allow us to determine the emittance dilution due to the BPM precision errors using eqs. (9) and (11). First, we use eq. (14), with the change $\delta \rightarrow \sigma$, to express Δx_σ,

$$\Delta x_\sigma \;=\; \Delta x_\sigma^{(1)} \;, \tag{16}$$

where we have only included the first order term since σ is assumed small. Next, we invert eq. (14) to solve for $\Delta x_\delta^{(1)}$ from the residual difference orbit Δx_δ

$$\Delta x_\delta^{(1)}(s) = \Delta x_\delta(s) - \sum_i \delta_i (KL)_i \Delta x_\delta(s_i) R_{12}(s, s_i) \quad . \tag{17}$$

Now, we need to relate $\Delta x_\sigma^{(1)}$ to $\Delta x_\delta^{(1)}$. The difference orbit Δx_δ is equal to the negative of the random BPM precision errors; it is constructed from sums of "deflections" and coefficients R_{12} which oscillate, eqs. (14) and (15). Thus, there are three length scales we need to consider: the length between "deflections" L_D, the betatron oscillation period L_β, and the length over which $\sigma(s)$ changes L_σ. Provided that L_D, $L_\beta \ll L_\sigma$, we can treat σ and δ as constant over the correlated "deflections". This allows us, using eq. (15) and performing ensemble averages over the random deflections, to find the relation:

$$\left\langle \Delta x_\sigma^{(1)^2} \right\rangle = \frac{\overline{\sigma^2}}{\delta^2} \left\langle \Delta x_\delta^{(1)^2} \right\rangle \ , \tag{18}$$

where $\overline{\sigma^2}$ is the average of $\sigma^2(s)$ over s. Now, using this result and eqs. (16) and (17), we find that after DF correction the BPM precision errors cause an RMS residual dispersive error of

$$\left\langle \Delta x_{\sigma\,\mathrm{BPM}}^2(s_f) \right\rangle = 2\sigma_{\mathrm{prec}}^2 \frac{\sigma^2}{\delta^2} + 2\sigma_{\mathrm{prec}}^2 \overline{\sigma^2} \sum_i (KL)_i^2 R_{12}^2(s_f, s_i) \quad . \tag{19}$$

To evaluate the sum in the second term in eq. (19), we need to assume a model linac. We use the model described in ref. [3], where the phase advance per cell is constant while the beta functions and the cell lengths increase with the square root of the beam energy. In addition, we assume that the energy spread of the beam decreases inversely with the beam energy. Using this model, we can evaluate the sum in eq. (19) by approximating it with an integral. In this manner, we find a dispersive error due to the BPM precision errors of

$$\left\langle \Delta x_{\sigma\,\mathrm{BPM}}^2(s_f) \right\rangle = 2\sigma_{\mathrm{prec}}^2 \frac{\sigma_0^2}{\delta^2} \frac{E_0}{E_f} + \frac{2}{3} \sigma_{\mathrm{prec}}^2 N_{\mathrm{BPM}} \overline{\beta_0}^2 (KL)_0^2 \sigma_0^2 \frac{E_0}{E_f} \quad . \tag{20}$$

Here, $\overline{\beta_0}$, $(KL)_0$, and σ_0 are the average beta function, the integrated quadrupole strength, and the energy spread at the beginning of the linac, and E_0 and E_f are the initial and final beam energies.

Finally, we can use eqs. (9) and (11) to solve for the chromatic emittance dilution due to this dispersive error. We will not perform the explicit substitutions here, but we will instead discuss a few implications of eq. (20). First, eq. (20) indicates that there will be a minimum dispersive error, due to the BPM precision errors, for some value of δ. The first term of eq. (20) decreases rapidly with δ while the second term remains constant; if we had included higher orders of δ, we would find terms that increase with δ. Secondly, notice that both terms in eq. (20) can be reduced by decreasing σ_{prec}, *i.e.*, the measurement error; the RMS of the BPM precision errors will tend to decrease with square root of the number of measurements when the separate measurements are averaged together. We will see this behavior in the results of simulations discussed in sec. 4.

3.3. Beam jitter

In a linac there are many sources of jitter which cause the beam position to fluctuate. For example, injection jitter, ground motion, and power supply fluctuations all have this effect. To prevent these from degrading the performance of a linear collider, this beam jitter must be constrained to be much less than the beam size; the beam jitter will directly increase the time average of the emittance since the beam changes position with time, thereby, increasing the effective phase-space volume occupied. In this section, we will estimate a secondary effect of the beam jitter, namely, its effect on the performance of the DF correction algorithm.

As was mentioned in sec. 2.2, the beam is most sensitive to dispersive errors when the beam energy spread is large. Thus, we will only consider jitter of the

injected beam, since the beam energy spread is typically largest at injection. Of course, if desired, our result could easily be generalized by summing over all the sources of the jitter. In fact, this will be done when analyzing the effect of magnet scaling errors which are treated in an analogous manner to the beam jitter errors.

In the case of injection jitter, the measured difference orbit will differ from the actual difference orbit by a betatron oscillation caused by the jitter in initial conditions. After correcting the measured difference orbit to zero, the actual difference orbit Δx_δ will be the negative of this betatron oscillation. To estimate the magnitude of Δx_σ, we use eqs. (16) and (17) derived in the previous section on the BPM precision errors. This case differs from the case of the BPM precision errors in that the deflections that create the difference orbit, *i.e.*, the summand of eq. (15), are only non-zero near the beginning of the linac. Thus, instead of eq. (18), we have the relation

$$\Delta x_\sigma^{(1)} = \mathrm{TA_X};\,) \text{ - -} \tag{21}$$

where σ_0 is the RMS energy spread at the beginning of the linac. Using this and eqs. (16) and (17), we find a dispersive error due to the beam jitter of

$$\left\langle \Delta x_{\sigma\mathrm{jit}}^2(s_f) \right\rangle = 2\sigma_{\mathrm{jit}}^2 \frac{\sigma_0^2}{\delta^2} + \left\langle \left(\sum_i \sigma_0 (KL)_i R_{12}(s_f, s_i) [\xi_0 R_{11}(s_i, s_0) + \xi_\delta R_{11}(\delta; s_i, s_0)] \right)^2 \right\rangle \quad , \tag{22}$$

where σ_{jit} is the RMS jitter measured at the *end* of the linac and the factor of two appears in the first term since two trajectories must be measured to calculate a difference orbit. The angle brackets denote an ensemble average over the jitter which is represented by ξ_0 for jitter of the on-energy trajectory and ξ_δ for

jitter of the trajectory after making the energy change of δ; note that for simplicity we have only included position jitter in these terms.

The expression in eq. (22) differs from the expression found for the BPM precision errors, eq. (19). The BPM precision errors are uncorrelated and thus the error $\langle \Delta x_\sigma{}^2 \rangle$ depends upon $N_{\rm BPM}$. In contrast, beam jitter leads to a difference orbit that oscillates like a betatron oscillation. Thus, the error due to the nonlinearity, the second term of eq. (22), will be correlated with the betatron phase advance and $\langle \Delta x_\sigma{}^2 \rangle$ will depend upon the square of $N_{\rm quad}$.

When performing the sums in eq. (22), we treat jitter of the on-energy trajectory and the off-energy trajectory separately because the induced betatron oscillations will have different phase advances; the phase advance is energy-dependent. In particular, after changing the effective beam energy, the different phase advance will cause the correlation between the injection error and the dispersive error to breakdown. Thus, we would find that jitter of the off-energy trajectory contributes far less than jitter of the on-energy trajectory; for this reason, we will only estimate the on-energy jitter.

Using the same model linac described in sec. 3.2, we can evaluate the sums in eq. (22) by approximating them with integrals. After DF correction, we find a dispersive error due to beam jitter of

$$\langle \Delta x_{\sigma_{\rm jit}}^2(s_f) \rangle \approx 2\sigma_{\rm jit}^2 \frac{\sigma_0^2}{\delta^2} + N_{\rm quad}^2 \frac{\sigma_{\rm jit}^2 \sigma_0^2}{32} (KL)_0^2 (\beta_{0\,\rm QF} - \beta_{0\,\rm QD})^2 \sqrt{\frac{E_0}{E_f}} \quad , \qquad (23)$$

where $N_{\rm quad}$ is the number of quadrupoles, $\sigma_{\rm jit}$ is the RMS beam jitter at the *end* of the linac, and $\beta_{0\,\rm QF}$ and $\beta_{0\,\rm QD}$ are beta functions at the focusing and defocusing magnets at the beginning of the linac.

One can solve for the chromatic emittance dilution due to this dispersive error using eqs. (9) and (11). As in the discussion of the BPM precision errors, we will

not perform the explicit substitutions here, but instead we will discuss eq. (23). Similar to the error due to the BPM precision errors, the first term of eq. (23) decreases rapidly with δ while the second does not, indicating that the residual error due to the beam jitter will have a minimum as a function of δ. Also, notice that, like the error due to the BPM precision errors, this contribution depends upon the measurement errors, and thus it can be reduced by averaging multiple measurements of the trajectory. We will estimate the effects of the beam jitter at the end of sec. 4, after discussing results from the simulations.

3.4. Magnetic scaling errors

Magnetic scaling errors occur when one changes the effective beam energy by scaling the magnetic fields. The errors arise because different magnets will scale slightly differently with the power supplies and because the power supplies have finite precision. Thus, one cannot reduce all of the magnetic fields by exactly the same percentage. Typically, it is possible to specify the magnetic field strength with an accuracy of roughly 10^{-3}.

The effect of these scaling errors is analogous to the effect of beam jitter. When measuring a difference orbit created by scaling the magnetic fields, one changes the fields, measures the off-energy trajectory, resets the magnets and measures the on-energy trajectory. We treat the final magnet values as the reference values and thus the scaling errors only cause errors when measuring the off-energy trajectory. We should emphasize that the order in which one measures the trajectories is important. If we measure the on-energy trajectory before the off-energy trajectory, the scaling errors would cause errors in both measurements.

If a magnet deflects the central trajectory by an angle θ and its magnetic field can be specified with an RMS accuracy of Δ, the off-energy trajectory will have an

RMS deflection error of $(1-\delta)\Delta\theta$. These deflections will drive betatron oscillations which will add to the measured difference orbit just as beam jitter does. After correction with the DF algorithm, the actual difference orbit will be corrected to the negative of this (off-energy) betatron oscillation. Thus,

$$\Delta x_\delta(s) = -\sum_i \Delta_i \theta_i R_{12}(\delta; s, s_i) \quad , \tag{24}$$

where we have neglected the factor $(1-\delta)$. Now, since the deflections $\Delta\theta$ are random, we can use eqs. (16), (17), and (18) to find Δx_σ. Using the model linac described earlier, we find a residual dispersive error of

$$\begin{aligned}\left\langle \Delta x_{\sigma\,\text{magnet}}^2(s_f)\right\rangle \approx N\frac{\langle\Delta^2\rangle\langle\theta_0^2\rangle}{\delta^2}\frac{\sigma_0^2\beta_0^2}{3}\frac{E_0}{E_f} \\ + \left\langle\left(\sum_i \sigma_i (KL)_i R_{12}(s_f, s_i)\sum_j^i \Delta_j\theta_j R_{12}(\delta; s_i, s_j)\right)^2\right\rangle .\end{aligned} \tag{25}$$

Here, N is the number of magnets and θ_0 is the deflection due to the magnets at the beginning of the linac. In addition, we have assumed that the deflection errors θ are random and that they decrease in strength inversely with the square root of the beam energy; this models quadrupole scaling errors in our example linac. In the case of quadrupole errors, θ is proportional to the integrated strength of the quadrupole and the distance of the trajectory from the magnetic center. Thus,

$$\langle\theta_0^2\rangle = (KL)_0^2\left(\langle y_m^2\rangle + \langle y_c^2\rangle\right) \quad , \tag{26}$$

where y_m and y_c are the RMS values of the quadrupole misalignments and the beam trajectory. Alternately, for dipole correctors, θ can be estimated by assuming a uniform distribution of kicks. Thus, $\langle\theta_0^2\rangle$ is equal to one-third of the initial peak deflection.

It is important to note that as described the magnet scaling errors only contribute to the error of the off-energy trajectory. The nonlinear term, *i.e.*, the second term of eq. (25), will be small because the off-energy phase advance differs from the on-energy phase advance and thus we can neglect it. A similar situation occurs in the case of beam jitter errors as discussed in the previous section. Of course, if the difference orbit is not measured using the procedure described at the beginning of this section, the magnet scaling errors could also affect the on-energy trajectory. In this case, eq. (25) would have a term proportional to $N \times N_{\rm quad}^2$; obviously this should be avoided.

Finally, we should note that the effect of the magnetic scaling errors does not depend upon measurement errors which can be reduced. Thus, these errors could limit the performance of our correction algorithm. In sec. 4.3 we will use eq. (25) along with eqs. (9) and (11) to estimate the magnitude of the errors; fortunately, they cause only a small error.

3.5. RF deflections

The RF is provided to accelerate the particles longitudinally. Unfortunately, there is typically a small coupling between the accelerating field and the transverse planes. The RF deflections present a problem for our algorithm because, unlike magnetic deflections, the RF deflections remain constant as the effective beam energy is changed. Thus, they cause the measured difference orbit to differ from the actual dispersive error.

The RF deflections are a sinusoidal function of the RF phase, typically offset in phase relative to the longitudinal acceleration:

$$E_{\rm acc} = E_{\rm RF}\cos\phi_0 \ , \qquad \theta_{\rm RF} = f\frac{E_{\rm RF}}{E(s)}\cos(\phi_0 - \phi_d) \ . \tag{27}$$

Here, f is the longitudinal-transverse coupling of the accelerating structure, $E_{\rm RF}$ is the energy gain from the structure, and $E(s)$ is the beam energy. In addition, ϕ_0 is the RF phase which equals zero for peak acceleration and ϕ_d is a phase offset.

There are two methods of changing the effective beam energy when measuring the difference orbit: one can either change the magnet strengths or the actual beam energy. For either method to work properly, all of the deflections should scale with the change in effective energy. Unfortunately, if one changes the magnet strengths, the RF deflections are not affected. Likewise, if one scales the RF to change the beam energy, the RF deflections also scale and the effect on the beam does not change.

Since the RF deflections do not change when varying the effective beam energy, the measured difference orbit will be independent of the RF deflections. The dispersive error in the beam resulting from the RF deflections and the beam energy spread can be directly calculated from eq. (14) with the substitution $\delta \rightarrow \sigma(s)$. Assuming that the RF errors are random and using the same model linac described earlier, we find a residual dispersive error of

$$\left\langle \Delta x^2_{\sigma {\rm RF}}(s_f) \right\rangle \approx \frac{N_{\rm RF}}{3} \langle f^2 \cos^2(\phi_0 - \phi_d) \rangle \sigma_0^2 \beta_0^2 \frac{E^2_{\rm RF}}{E_f E_0} \sqrt{\frac{E_0}{E_f}} \quad . \tag{28}$$

Here, $N_{\rm RF}$ is the number of accelerator sections.

Notice that the RF errors do not depend upon the effective energy change δ used to create the difference orbit. Furthermore, this effect cannot be reduced by making multiple measurements of the trajectory. Thus, the RF errors could provide a serious limitation on the performance of the correction algorithm. We will use eq. (28) along with eqs. (9) and (11) to estimate the importance of these errors in both the SLC and NLC linacs after describing the results of the simulations in sec. 4.

4. Examples

We have written a computer program to test the DF correction technique against the one-to-one correction algorithm. The program simulates random transverse misalignments of the quadrupoles and BPMs, random quadrupole strength errors, and BPM precision errors. We have not included effects due to RF deflections or beam jitter; these are discussed in sec. 4.3 using the results of sec 3. In addition, we have not included the effects of wakefields; this is a subject of continuing research [8]. Finally, we have tested our algorithm on two lattices: a preliminary design of the NLC [2] linac and the current lattice for the SLC linac.

4.1. The NLC

The NLC main linac will accelerate bunches from 16.5 GeV to 250 GeV. Our preliminary lattice is composed of 210 simple FODO cells with a phase advance of 90 degrees. The cell lengths are scaled as $\sqrt{E(s)}$ so that the phase advance per cell remains constant while the beta functions increase with the square root of the beam energy [3]. Figure 1 contains a plot of the horizontal and vertical beta functions; the square root of a beta function is proportional to the RMS beam size. The center of the plot shows the locations of the horizontally focusing and defocusing quadrupoles. Figure 2 shows the energy profile in the linac and the relative RMS energy spread σ_ϵ of the bunch. The bunch is assumed to have an RMS energy spread of 1.0% at the beginning of the linac; this then decreases inversely with the energy as the bunch is accelerated. We have not included the energy spread induced by the longitudinal wakefields or the energy spread which is used by the BNS damping [8] technique to reduce the effect of wakefields. Finally, the beam emittances in the NLC are $\gamma\epsilon_x = 3 \times 10^{-6}$mrad and $\gamma\epsilon_y = 3 \times 10^{-8}$mrad , and the beam size at the end of the linac is roughly 10 μm $\times$ 1 μm.

To simulate correcting the orbit in the NLC, we use twenty different sets of random errors. The errors are found from gaussian distributions which have been cutoff at two sigma; the RMS values of the errors are listed in table 1. The quadrupoles are misaligned 70 μm relative to the linac centerline and the BPMs are misaligned 70 μm *relative* to the quadrupoles; thus, the BPMs are misaligned with an RMS of roughly 100 μm relative to the linac centerline. The BPM precision errors of 2 μm are estimated assuming that a measurement precision the order of the beam size will be achieved in the NLC. Finally, the quadrupole strength errors are constant, simulating calibration errors; the errors do not change from measurement to measurement as power supply fluctuations would.

The trajectory is corrected in the NLC by moving the quadrupoles horizontally or vertically to achieve the desired deflection. We use both the focusing and defocusing quadrupoles for correction. When correcting with the DF algorithm, the linac is divided into eleven sections, each containing twenty cells. We then use the algorithm to correct each section instead of correcting the entire linac at once. While correcting the linac in sections will not minimize the dispersion as well as correcting the entire linac at once, this procedure reduces the sensitivity to discrepancies between the machine and the model one uses for correction. In all cases, we calculate a solution with a single iteration of the DF algorithm.

Results from correcting the twenty sets of errors with the two correction schemes are listed in table 2; the error on the data is equal to one standard deviation. The Orbit RMS data is the RMS of the trajectory relative to the linac centerline, while the BPM RMS data is the RMS of the BPM measurements. Notice that the one-to-one algorithm zeros the BPM readings (within the BPM precision) while the actual trajectory is relatively large. In contrast, our method corrects both the actual trajectory and the measured BPM readings. In fact, the DF correction

algorithm does better correcting the actual trajectory than does the one-to-one method.

Of course, we are not only interested in correction of the trajectory. The dilution of the vertical emittance due to the dispersive errors is listed in the bottom row of table 2; the magnification of the horizontal emittance will be much smaller than the vertical since the initial emittance is one hundred times larger. Obviously, the one-to-one correction technique leads to a large (factor of seven) increase in the vertical emittance. Furthermore, this emittance will continue to filament and thus the effective emittance growth may be much larger. In contrast, the new technique performs very well, virtually eliminating the chromatic dilution.

The difference in correction techniques is illustrated in figs. 3–5. Figure 3 compares the trajectory after DF correction (upper plot) with the result of one-to-one correction (lower plot) and fig. 4 compares the BPM readings in the same manner. One can see that the one-to-one method zeroes the BPMs, but does not correct the actual trajectory as well as the DF method. Finally, fig. 5 shows the *difference* between the trajectory of an on-energy particle and a particle whose energy differs from the design, the energy difference being equal to the RMS energy spread shown in fig. 2; this is the difference orbit Δx_σ — eq. (10). Obviously, the dispersive error, *i.e.*, this difference orbit, and therefore the chromatic dilution, is much smaller in the case of the DF correction.

It is evident from table 2 that the DF correction technique performs substantially better that the one-to-one method. In all of the data shown, the effective energy change used by the DF algorithm was $\Delta E/E = 10\%$. Changing the beam energy, or equivalently changing the magnet strengths, is not necessarily easy and can in itself introduce errors. For this reason, we wish to limit the energy change used by the correction algorithm. Unfortunately, as the energy difference is decreased, the measurement of the difference orbit, used by the DF algorithm, will be

lost in the noise of the BPM precision errors, and thus the correction technique will not perform as well.

In fig. 6 we plot results of the DF correction technique, again found from the correction of twenty sets of random errors, versus the change in effective energy $\Delta E/E$. There are three curves: the dotted is the emittance magnification which has a scale on the right, the solid is the RMS of the trajectory, and the dashed curve is the RMS of the BPM measurement of the trajectory. Notice that both the emittance magnification and the RMS of the trajectory have broad minimums. The increase which occurs as $\Delta E/E$ increases is due to the nonlinearity of the dispersion. In contrast, as $\Delta E/E$ decreases, the BPM precision errors reduce the effectiveness of the algorithm. Our estimate eq. (20) is in good agreement with both the behavior and the magnitude of this residual error. Finally, one can reduce the error due to the BPM precision errors by making multiple readings of the BPMs. For example, if we read the BPMs three times to make each measurement, the BPM precision error should decrease from 2.0 μm to 1.2 μm. In this case, we verified that the emittance dilution decreases by almost a factor of three as expected.

Finally, in fig. 7, we plot the result of the DF correction technique versus the magnitude of the BPM precision errors which are varied from 2 μm to 40 μm. As before, the data was found from the correction of twenty sets of random errors. As in fig. 6, the three curves: solid, dashed, and dotted, are the actual trajectory RMS, the measured trajectory RMS, and the vertical emittance dilution; the first two curves have scales on the left and the emittance dilution has a scale on the right side of the plot. Notice that the emittance dilution is still less than 25% when the BPM precision errors have been increased to 8 μm, which is roughly eight times the vertical beam size. Also notice that the RMS of actual trajectory decreases rapidly as the magnitude of the BPM precision errors is decreased. In fact, the decrease

in the trajectory RMS, which is important for controlling wakefield effects, may be the most significant gain from decreasing the BPM precision errors.

4.2. The SLC

The SLC linac accelerates bunches from 1.153 GeV to roughly 50 GeV. The beta functions for the lattice are plotted in fig. 8. Notice that the quadrupole spacing is increased in two steps from an initial spacing of three meters to a spacing of twelve meters. The RMS energy spread due to the initial energy spread of 1.0% is plotted in fig. 9. In addition, BNS damping [9] is used in the SLC linac to control the wakefields, which are significant. In fig. 10, we have plotted the energy spread in the beam when using BNS damping [10] with a bunch of roughly $2 \times 10^{10} e^-$. The correlated energy spread, added when running with BNS damping, is used to cancel the transverse wakefield effects. Thus, this additional energy spread should not contribute to the chromatic dilution. Of course, the cancellation is not local and thus the actual chromatic dilution should be between the results found from energy spreads with and without BNS damping. Finally, the SLC is designed to operate with emittances of $\gamma\epsilon_x = \gamma\epsilon_y = 1.5 \times 10^{-5}$mrad in the collider mode and $\gamma\epsilon_x = 3 \times 10^{-5}$mrad and $\gamma\epsilon_y = 3 \times 10^{-6}$mrad in the flat beam mode. Thus the beam sizes are roughly 80 μm $\times$ 80 μm in the collider mode and 110 μm $\times$ 35 μm in the flat beam mode. We will see that the chromatic dilution is not very significant in the colliding beam mode, but, because of the smaller vertical beam size, it is more important for the flat beams.

As was done with the NLC, we simulated correcting the orbit in the SLC with twenty different sets of random errors. The errors used are listed in table 1 along with those used for the NLC. Specifically, we used RMS values of 150 μm for the quadrupole and BPM transverse misalignments; as before, the quadrupoles were

misaligned relative to the linac centerline while the BPMs were misaligned relative to the quadrupoles. These errors are thought to be similar in magnitude to the errors in the current machine. In addition, we assumed 0.1% quadrupole strength errors and BPM precision errors with an RMS of 15 μm. The measured BPM precision in the SLC is 25 μm, but the 15 μm precision can be achieved by reading each BPM three times when measuring the trajectory.

In contrast to the NLC, in the SLC the orbit is corrected using dipole correctors located near the focusing quadrupoles. We used only the correctors and BPMs which are actually used for orbit correction; a number are set aside for various feedback systems. Finally, as was done with the NLC, we divided the SLC into six sections of roughly twenty cells which were then corrected individually.

The results of the two correction techniques, including errors of one standard deviation, are listed in table 3. As before, the Orbit RMS is the RMS of the trajectory relative to the linac centerline, and the BPM RMS is the RMS of the BPM measurements. Notice that the one-to-one algorithm does not zero all of the BPMs; only BPMs located at the focusing quadrupoles are zeroed. Again, note that the new algorithm improves the actual trajectory without improving the measured trajectory.

The middle two rows of table 3 list the emittance magnification when in the colliding beam mode. The upper row does not include the energy spread used for BNS damping, while the lower does. These magnifications are listed in units of the initial normalized emittance of 1.5×10^{-5} mrad . We see that there is a small dilution of the emittance even when using the one-to-one algorithm. The bottom two rows list the vertical emittance magnification when running in the flat beam mode: $\gamma\epsilon_{y0} = 3 \times 10^{-6}$ mrad . Notice that the fractional increase of the emittance has increased by roughly a factor of four. This occurs because the flat beam vertical emittance is roughly five times smaller than the colliding beam emittances.

Again, the difference in correction techniques is illustrated in Figs. 11–13. Figure 11 compares a trajectory after DF correction (upper plot) with the result of one-to-one correction (lower plot) and fig. 12 compares the BPM readings in the same manner. Finally, fig. 13 is a plot of the difference between the trajectory of a particle with the design energy and a particle whose energy differs from the design by the BNS energy spread shown in fig. 10. As before, the DF correction results, for both the trajectory and the chromatic dilution, are better than the one-to-one correction results.

Despite the fact that we do not find significant degradation of the colliding beam emittance as a result of chromatic dilution, the dispersive errors still present difficulties. One example is the energy management system. When one klystron fails, another turns on, maintaining the beam energy. Typically, the spare klystron is located at the end of the machine. Thus, the beam energy changes by roughly 200 MeV, the energy gain from one klystron, between the failed klystron and the replacement. If the klystron fails near the beginning of the linac, this energy change can lead to a very large orbit change. The RMS trajectory changes for a few examples are listed in table 4. In the SLC, there are eight klystrons per sector and twenty-nine sectors. The sectors are numbered 2 thru 30, from the damping ring to the end of the linac. The klystrons are labeled by their sector number and then the number within the sector. Thus, klystron 2–8 sits at the end of sector 2 and is near the beginning of the machine. As one can see from table 4, changing a klystron near the beginning of the machine leads to a large orbit change, roughly 100 μm RMS. In contrast, the DF correction method, by correcting the chromatic dependence of the trajectory, reduces the orbit shift by an order of magnitude.

Finally, as in the NLC example, all data from the DF correction algorithm was calculated with an effective energy difference $\Delta E/E = 10\%$. We illustrate the

dependence of the correction on $\Delta E/E$ in fig. 14. Again, we plot three curves: the dotted is the emittance magnification which has a scale on the right, the solid is the RMS of the trajectory, and the dashed curve is the RMS of the BPM measurement of the trajectory. Notice that the plot looks similar to fig. 6, the $\Delta E/E$ dependence of the DF correction technique in the NLC.

4.3. Errors

In this section we estimate the effects of errors not included in the simulations. Specifically, we discuss the effect of beam jitter, RF deflections and magnetic scaling errors. Because these effects are machine specific, we will discuss the SLC and the NLC linacs separately.

4.3.1. The SLC

In the SLC, the transverse-longitudinal coupling of the RF structures f is estimated in ref. [11] to have an RMS of $f = 4 \times 10^{-4}$. Each three meter accelerator section has an energy gain of roughly 60 MeV. Assuming that the effective energy change is made by scaling the magnet strengths and using eq. (28), we estimate an error of

$$\Delta x_{\sigma \mathrm{RF}} \approx 1.6\,\mu\mathrm{m} \qquad (\mathrm{SLC}) \quad . \tag{29}$$

This residual dispersive error is much less than the RMS beam size and can therefore be neglected. In fact, such an error would increase the vertical emittance of a flat beam in the SLC by roughly 0.1%. We should note that the model linac used to derive eq. (28) is not an exact model of the SLC linac, but modifying the model will not change the result too much; at most a factor of two.

If instead, the energy change was achieved by changing the beam energy, we would find a result even smaller *except* for the kicks due to the large changes in the first few RF sections. The large initial changes are needed to shift the initial beam energy by the desired amount; all subsequent changes are incremental and are therefore smaller. Turning a single klystron off, each of which powers four accelerator sections, could lead to an error of roughly 100 μm. Obviously, this is not tolerable.

Now, we estimate the effects of magnet scaling errors. We will assume a random 1% absolute error of the magnetic field strength after scaling the magnets. If the effective energy were changed by 10%, this would correspond to a 10% relative error in the scaling. Using eq. (25), we find

$$\Delta x_{\sigma\,\mathrm{magnet}} \approx 2.1\,\mu\mathrm{m} \quad , \tag{30}$$

where we have combined the results from both the correctors and the quadrupoles. Again, we can neglect the error since it is much smaller than the RMS beam size.

Finally, we consider the effect of beam jitter. For a worst case estimate, we will assume all of the jitter is due to injection jitter. If the jitter is 25% of the vertical beam size, $\sigma_{\mathrm{jit}} = 9\ \mu$m, we find using eq. (23)

$$\Delta x_{\sigma\,\mathrm{jitter}} \approx\ 7.8\,\mu\mathrm{m} \quad , \tag{31}$$

when the effective energy change δ is 10%. This is still much smaller than the beam size and would only cause an emittance dilution of roughly 2%.

4.3.2. The NLC

In the NLC, we estimate the effect of the RF deflections using the same transverse-longitudinal coupling f as was measured in the SLC: $f = 4 \times 10^{-4}$. We further assume that the accelerator sections in the NLC are one meter in length and each gives an energy gain of 100 MeV. In this case, eq. (28) yields an estimate of

$$\Delta x_{\sigma \mathrm{RF}} \approx 0.3\,\mu\mathrm{m} \qquad \text{(NLC)} \quad . \tag{32}$$

This residual dispersive error is comparable to the NLC vertical beam size. Using eqs. (9) and (11), we find that it would lead to an emittance increase of roughly 5%. Of course, the actual tolerances on the RF accelerator sections in the NLC would likely be tighter than those in the SLC. If the tolerance on the transverse-longitudinal coupling were reduced from $f = 4 \times 10^{-4}$, this error should not be significant; the residual dilution scales with the square of f.

We also estimate the effect of the magnetic scaling errors using the same error as was used in the SLC, namely, random 1% absolute errors of the magnetic field strengths after scaling the magnets by 10%. Using eq. (25), we find

$$\Delta x_{\sigma \mathrm{magnet}} \approx 0.5\,\mu\mathrm{m} \quad . \tag{33}$$

This causes a 13% emittance dilution. Of course, again, we believe that we have overestimated the error. In principle, one could reduce the absolute scaling error to 0.1% by cycling the magnets on a specified path through their hysteresis curves. In this case the chromatic dilution would be negligible.

Next, we consider the effect of beam jitter. As in the SLC case, we estimate the effect of injection jitter that is 25% of the vertical beam size. Using eq. (23), we find

$$\Delta x_{\sigma\text{jitter}} \approx 0.3\,\mu\text{m} \qquad \text{(NLC)} \quad , \tag{34}$$

when using an effective energy change of 10%. This error causes an emittance dilution of 4%.

Finally, to verify our estimates, we simulated both random magnetic scaling errors and jitter of the injected beam. Random 1% absolute errors were added to the magnetic fields strengths when scaling the magnets by 10%. We found an emittance dilution of 10.0±8.7% due to the scaling errors; this is in fairly good agreement with our estimate of 13%.

The injection jitter was simulated by adding a random initial position offset to the trajectories used to measure the difference orbit; the position offsets have an RMS equal to 25% of the initial beam size. In this case, we found an emittance dilution of $3.1 \pm 1.9\%$ when making an effective energy change of 10%. Again, this is in good agreement with our estimate of 4%.

5. Alternate Techniques

Although the DF correction technique improves both the chromatic dilution and the trajectory, it is not necessarily easy to implement. Thus, we will compare with an alternate method of chromatic correction. Here, a closed bump is used to pass the beam off-center through a quadrupole. This will then cause a dispersive error. By using such a bump in conjunction with a spot size monitor, the ***linear*** part of the dispersion can be cancelled. Of course, one needs two bumps and beam size monitors to correct both the beam size and divergence.

This bump technique and the DF correction techniques are similar in that both use trajectory displacements in the quadrupoles to correct the dispersive error; the two methods differ in that the DF method corrects the dispersion locally while the bump method corrects the error at a discrete location. The advantage of the bump method is that it is not sensitive to errors such as RF deflections or jitter tolerances. The disadvantage is that it only corrects the linear portion of the dispersion at a single location.

Figure **15** is a plot of the *y-p,* phase-space at the end of the NLC linac after correction with the one-to-one trajectory correction algorithm; the error distribution was one of those described in sec. 4.1. The curve plots the endpoints of particle trajectories having energies between $+\sigma_\epsilon$ and $-\sigma_\epsilon$. Also, for reference, the RMS beam size, excluding the dispersive error, is plotted about the design energy trajectory. Obviously, there is a large chromatic dilution in fig. 15. The emittance magnification is estimated to be 8.5 using eq. (11), although the magnification is actually larger that a factor of nine; reasons for this discrepancy are discussed in sec. 2.4. The important issue, illustrated in fig. 15, is that the dispersion is highly nonlinear and thus the bump method cannot correct a large fraction of the error.

We can calculate the optimal linear corrections by integrating, in the y–p_y phase-space, the energy-dependence of the trajectory:

$$\begin{aligned} Y_c(\sigma_\epsilon) &= \frac{1}{\sigma_\epsilon\sqrt{2\pi}} \int d\delta e^{-\delta^2/2\sigma_\epsilon^2} \frac{\delta}{\sigma_\epsilon} Y(\delta) \\ Y_c'(\sigma_\epsilon) &= \frac{1}{\sigma_\epsilon\sqrt{2\pi}} \int d\delta e^{-\delta^2/2\sigma_\epsilon^2} \frac{\delta}{\sigma_\epsilon} Y'(\delta) \quad . \end{aligned} \tag{35}$$

The optimal corrections for the dispersion in fig. 15 are listed in table 5. We have calculated the corrections for the portion of the beam with energies between $\pm\sigma_\epsilon$, $\pm 2\sigma_\epsilon$, and $\pm 3\sigma_\epsilon$; the first corresponding to just the core of the beam while the

later cases include the tails of the distribution. When correcting just the core, the correction reduces the magnification from a factor of nine to a factor of five; the correction is even worse when we include the tails of the distribution. Obviously, this is insufficient.

One solution is to place many bumps and beam size monitors along the linac, correcting the dispersion before the nonlinear terms become significant. Figure 16 is a plot of the dispersive error after roughly the first sixth of the NLC linac, $s = 550$ meters; the our version of the linac is 2925 meters long. While one can see that emittance dilution is not as large as in fig. 15, the dispersive error is still nonlinear. Again, we calculated the optimal linear corrections which could be obtained using the bump method; these results are listed in table 6. One can still see that this correction is not sufficient for the NLC.

Finally, fig. 17 is a plot of the *y-p,* phase-space at the end of the NLC after DF correction. This should be compared with fig. 15, which is the same phase-space, although with different scales, after one-to-one correction. Here, the emittance magnification is quite small, roughly a factor of 1.011. By using the bump method in addition to DF correction, the dilution can be decreased by a factor of two to 5%. While this additional correction is not necessary in this case, the bump method can provide additional correction if the nonlinearity, RF deflections, or magnetic scaling errors degrade the performance of the DF correction technique.

6. Tolerances

When designing a high energy linac, transverse alignment tolerances are specified to limit both wakefield effects and the chromatic dilution of the beam emittance. In the SLC linac, wakefields are a much greater limitation, at the operating beam current, than the chromatic effects. The chromatic effects are small since

the misalignments of the BPMs and quadrupoles are the order of the beam size. In the NLC, wakefield effects will be smaller (by design). Thus, if uncorrected, the chromatic dilutions could determine the alignment tolerances.

The scaling of the emittance dilution with the misalignments was discussed in sec. 2.4. After correcting the trajectory with the one-to-one technique, the dilution depends quadratically upon the magnitude of the misalignments when the dilution is small, less than 100%. As the emittance dilution increases, the dependence becomes a linear function of the misalignment magnitude. In contrast, the dilution when correcting with the DF technique is roughly independent of the misalignment magnitude. We have removed this dependence by scaling the trajectory measurements in eq. (6) by the estimated RMS of the misalignments. Thus, the emittance dilution should only depend upon the other errors, namely, BPM precision, beam jitter, magnet scaling errors, and the RF deflections; these effects were discussed in sec. 3 and were estimated for the SLC and NLC linacs in sec. 4.3 using eqs. (20), (23), (25), and (28). Actually, the dilution is weakly dependent upon the misalignment magnitude since the chromatic correction is not exactly local; trajectory errors in the last few magnets will lead to a small chromatic dilution that depends upon the magnitude of the trajectory and thus the magnitude of the misalignments.

The dependence of the trajectory correction techniques on the misalignment amplitude is illustrated in fig. 18. Here, we have varied the RMS magnitude of the vertical BPM and quadrupole misalignments from 7 μm to 350 μm; note that all of the axes in fig. 18 have logarithmic scales. The points plotted were found from the average of correcting twenty sets of random errors. The solid and dashed lines, at the top of the plot, are the RMSs of the actual trajectory after correction with the one-to-one and DF techniques, respectively; these curves have scales on the

left side of the figure. The DF technique is slightly better at correcting the actual trajectory, but the two curves are similar; in both cases the RMS of the trajectory is roughly proportional to the RMS of the misalignments.

The two other curves, the dotted and the dot-dash lines, are the emittances after correction with the one-to-one and DF techniques. The dilution after one-to-one correction is strongly dependent upon the misalignment magnitude. Here, the dilution varies from roughly 25% to over 3400% as the misalignments increase. In contrast, the dilution after DF correction is only weakly dependent upon the misalignment magnitude; it increases slowly from roughly 1% to 6% of the initial emittance as the misalignments become larger.

Thus, when using the DF correction technique, the chromatic dilution is effectively uncoupled from the magnitude of the transverse magnet misalignments. The transverse magnet alignment tolerances then need to be determined by other effects such as wakefields which, in many future linear collider designs, impose looser tolerances on the magnet alignment than the uncorrected chromatic dilution. Instead, the DF correction technique imposes relatively straight-forward tolerances on the BPM precision, beam jitter, RF deflections, and magnet scaling.

7. Summary

In this paper, we have described a new trajectory correction algorithm for linear accelerators that reduces the chromatic dilution of the transverse emittance while correcting the trajectory. The chromatic dilution arises because the beam is deflected due to stray fields and misalignments. Roughly, the dilution scales with the size of the misalignments relative to the beam size. Future linear collider designs tend to have very small beams to achieve the necessary luminosity, and thus,

if uncorrected, the chromatic dilution would impose extremely tight alignment tolerances in these future machines.

We have demonstrated the effectiveness of our technique in simulations of both the SLC and NLC linacs while comparing with the results of a standard correction technique, the one-to-one algorithm. In all cases, the DF correction algorithm reduced the chromatic dilution substantially while correcting the trajectory as well or better than the one-to-one algorithm. While the simulations indicate that chromatic dilution should not seriously degrade the performance of the SLC linac, the dilution will be debilitating in the NLC. Specifically, we found that with 70 μm misalignments in the NLC, the one-to-one algorithm causes roughly a 700% increase in the initial vertical emittance of $\gamma\epsilon_y = 3 \times 10^{-8}$ mrad . In contrast, the DF correction algorithm reduced this chromatic dilution to a few percent.

In addition, we have estimated the effect of errors not included in the simulations, with the exclusion of wakefields. The primary causes of additional error are beam jitter, RF deflections and scaling errors of the magnets. Our estimates show that in the NLC these effects should not seriously degrade the algorithm's performance.

Although we have not include wakefield effects in the simulations, they should, by design, be a smaller effect in the NLC. Of course, this is not true in the SLC linac. Regardless, wakefield effects are beyond the scope of this report. Obviously, they should be included in future research [8].

Finally, we have compared our correction algorithm with another technique of correcting the chromatic dilution that corrects the dilution at a discrete location. Unfortunately, the dispersion is highly nonlinear and since this method can only correct the linear portion of the error, it does not perform very well. Similarly, our technique only cancels the linear portion of the dispersive error, but it performs

very well since it corrects the errors locally, before the energy-dependent phase advance adds significant nonlinearities.

To conclude, we believe that our algorithm can effectively control the chromatic dilution in a linear accelerator while correcting the trajectory. It is important to note that with our method the chromatic dilution is roughly independent of the magnitude of the misalignments; the dilution depends upon the BPM precision errors and the magnitude of the magnet and RF scaling errors. This will be especially important for future linear colliders where it may be unreasonable to specify extremely tight transverse alignment tolerances for a multikilometer linac.

References

[1] See for example: J.D. Lawson, The Physics of Charged Particle Beams (Clarendon Press, Oxford, England, 1988); D.C. Carey, The Optics of Charged Particle Beams (Harwood Academic, Chur Switzerland, 1987); or S. Humphries, Jr., Charged Particle Beams (Wiley, N.Y., 1990).

[2] The NLC is a 250 GeV on 250 GeV linear collider being studied at SLAC. Some information can be found in ref. 3. More detailed parameters can be found in both: Proc. DPF Summer Study, Snowmass '88 and Proc. Int. Workshop on Next-Generation Linear Colliders, SLAC–335 (1988).

[3] R.D. Ruth, "Beam Dynamics in Linear Colliders," Proc. XIV Int. Conf. on High Energy Accelerators, Tsukuba, Japan, 1989; and SLAC–PUB–5091 (1989).

[4] C.E. Adolphsen *et al.,* "Beam–Based Alignment Technique for the SLC Linac," Proc. IEEE Part. Acc. Conf., Chicago, 1989; and SLAC–PUB–4902 (1989).

[5] T.L. Lavine, et al., " Beam Determination of the Quadrupole Misalignments and Beam Position Monitor Biases in the SLC Linac," Proc. 1988 Linear Acc. Conf., Williamsburg, Virginia, 1988; and SLAC–PUB–4720 (1988).

[6] E.D. Courant and H.S. Snyder, "Theory of the Alternating-Gradient Synchrotron," Annals of Phys., **3** (1958) 1.

[7] M. Sands, "The Physics of Electron Storage Rings," SLAC–121 (1971).

[8] T. O. Raubenheimer, work in progress.

[9] V. Balakin, A. Novokhatsky, and V. Smirnov, Proc 12th Int. Conf. on High Energy Accelerators, Fermilab, (1983), p. 119.

[10] This energy spread was calculated for a bunch of $2 \times 10^{10} e^-$ in the SLC by Karl Bane of SLAC. The energy spread will be increased as the bunch population is increased to the goal of roughly 5×10^{10}.

[11] J. Seeman, "Effects of RF Deflections on Beam Dynamics in Linear Colliders," Proc XIV Int. Conf. on High Energy Accelerators, Tsukuba, Japan, 1989; and SLAC–PUB–5069 (1989).

Table 1
Errors in the NLC and SLC lattices

	NLC	SLC
Quadrupole misalignments	70 μm	150 μm
BPM misalignments	70 μm	150 μm
Quadrupole strength	0.1%	0.1%
BPM precision	2.0 μm	15 μm

Table 2
Correction in the NLC

	One–to–One	DF
Orbit RMS	$89 \pm 3 \quad \mu$m	$54 \pm 3\,\mu$m
BPM RMS	$3 \pm 0.5\,\mu$m	$80 \pm 3\,\mu$m
Magnification of ϵ_y	$7.20 \pm 3.2\,\epsilon_{y0}$	$1.02 \pm 0.02\,\epsilon_{y0}$

Table 3
Correction in the SLC

	One–to–One	DF
Orbit RMS	$156 \pm 14\ \mu$m	$83 \pm 8\ \mu$m
BPM RMS	$154 \pm 11\ \mu$m	$184 \pm 8\ \mu$m
Magnification of ϵ (colliding beams, no BNS)	$1.01 \pm 0.01\ \epsilon_0$	$1.00 \pm 0.00\ \epsilon_0$
Magnification of ϵ (colliding beams with BNS)	$1.15 \pm 0.13\ \epsilon_0$	$1.00 \pm 0.00\ \epsilon_0$
Magnification of ϵ_y (flat beams, no BNS)	$1.04 \pm 0.04\ \epsilon_{y0}$	$1.00 \pm 0.00\ \epsilon_{y0}$
Magnification of ϵ_y (flat beams with BNS)	$1.67 \pm 0.60\ \epsilon_{y0}$	$1.00 \pm 0.00\ \epsilon_{y0}$

Table 4
Klystron changes in the SLC

Klystron		One–to–One	DF
2–8 Off	29–3 On	$95 \pm 37\,\mu$m	$9 \pm 6\ \ \mu$m
6–3 *Off*	30–1 On	$31 \pm 12\,\mu$m	$3.2 \pm 0.9\,\mu$m
15–7 Off	29–1 On	$23 \pm 7\ \ \mu$m	$1.8 \pm 0.5\,\mu$m

Table 5
Linear chromatic corrections for the phase space in fig. 15

	Eq. (11)	$\pm\sigma_\epsilon$	$\pm 2\sigma_\epsilon$	$\pm 3\sigma_\epsilon$
Uncorrected ϵ magnification	8.49	9.14	9.22	9.26
Corrected ϵ magnification		5.02	7.16	7.55
Correction $Y_c(\sigma_\epsilon)$		1.12 μm	$-0.52\,\mu$m	$-1.37\,\mu$m
Correction $Y_c'(\sigma_\epsilon)$		0.69 μrad	0.53 μrad	0.46 μrad

Table 6
Linear chromatic corrections for the phase space in fig. 16

	Eq. (11)	$\pm\sigma_\epsilon$	$\pm 2\sigma_\epsilon$	$\pm 3\sigma_\epsilon$
Uncorrected ϵ magnification	5.46	5.64	5.31	5.32
Corrected ϵ magnification		2.52	3.96	4.65
Correction $Y_c(\sigma_\epsilon)$		$-1.46\,\mu$m	$-0.83\,\mu$m	$-0.40\,\mu$m
Correction $Y_c'(\sigma_\epsilon)$		$-1.24\,\mu$rad	$-0.88\,\mu$rad	$-0.65\,\mu$rad

Figure Captions

1. NLC lattice.

2. NLC Energy Profile.

3. Actual trajectory in the NLC after

   (a) DF correction and

   (b) one-to-one correction.

4. BPM measurements in the NLC after

   (a) DF correction and

   (b) one-to-one correction.

5. Difference orbit in the NLC after

   (a) DF correction and

   (b) one-to-one correction.

6. DF correction versus the energy change $\Delta E/E$.

7. DF correction versus the BPM precision errors.

8. SLC lattice.

9. SLC energy profile without BNS damping.

10. SLC energy profile with BNS damping.

11. Actual trajectory in the SLC after

    (a) DF correction and

    (b) one-to-one correction.

12. BPM measurements in the SLC after

    (a) DF correction and

    (b) one-to-one correction.

13. Difference orbit in the SLC after

    (a) DF correction and

    (b) one-to-one correction.

14. DF correction versus the energy change $\Delta E/E$.

15. The y–p_y phase-space at the end of the NLC after one-to-one correction.

16. The y-p, phase-space at $s = 550$ m in the NLC after one-to-one correction.

17. The y–p_y phase-space at the end of the NLC after DF correction.

18. One-to-one and DF correction versus the RMS misalignment magnitude.

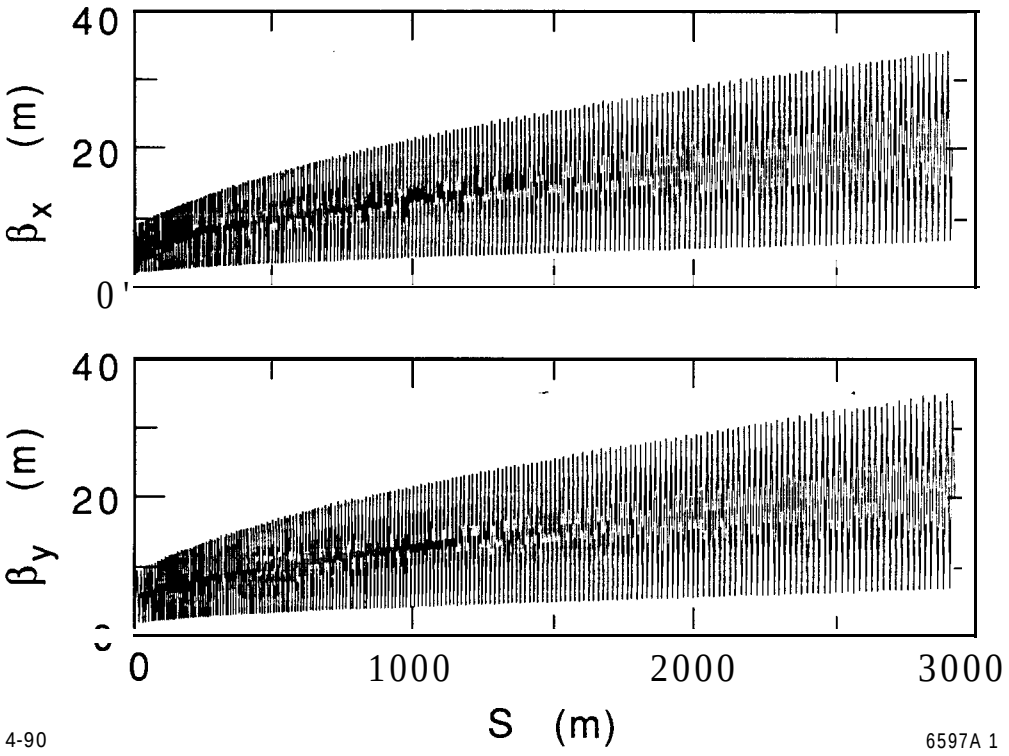

Fig. 1

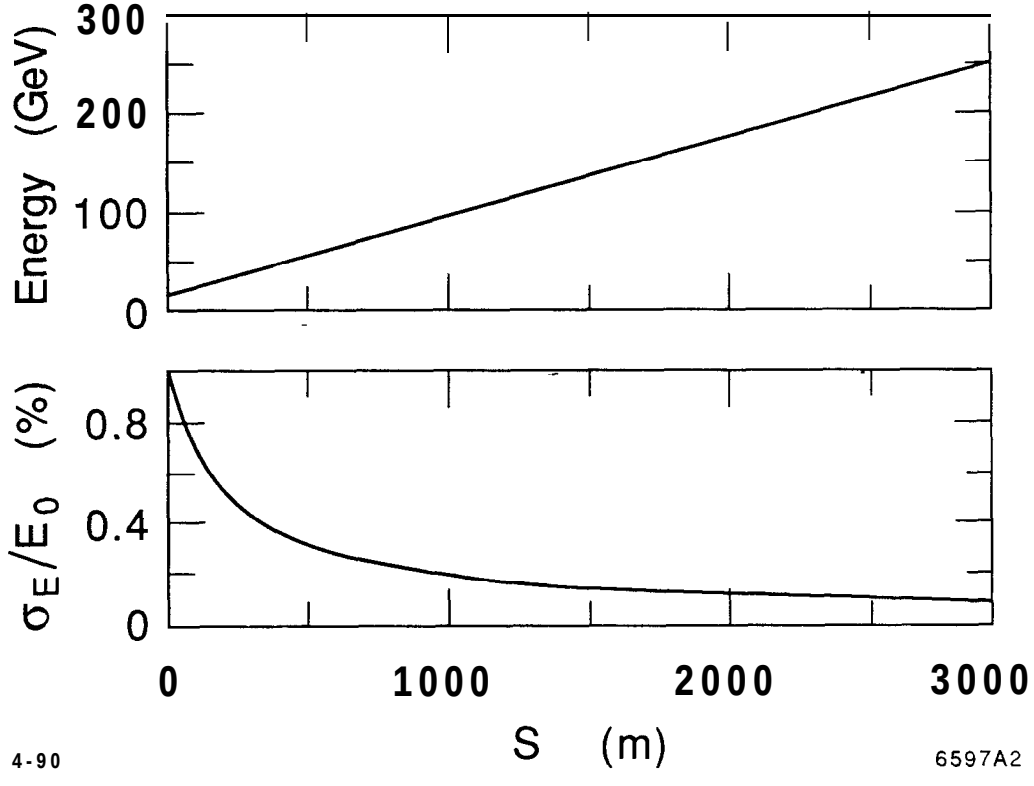
300
200
100
0
Energy (GeV)
0.8
0.4
0
σ_E/E_0 (%)
0
1000
2000
3000
S (m)
4-90
6597A2

Fig. 2

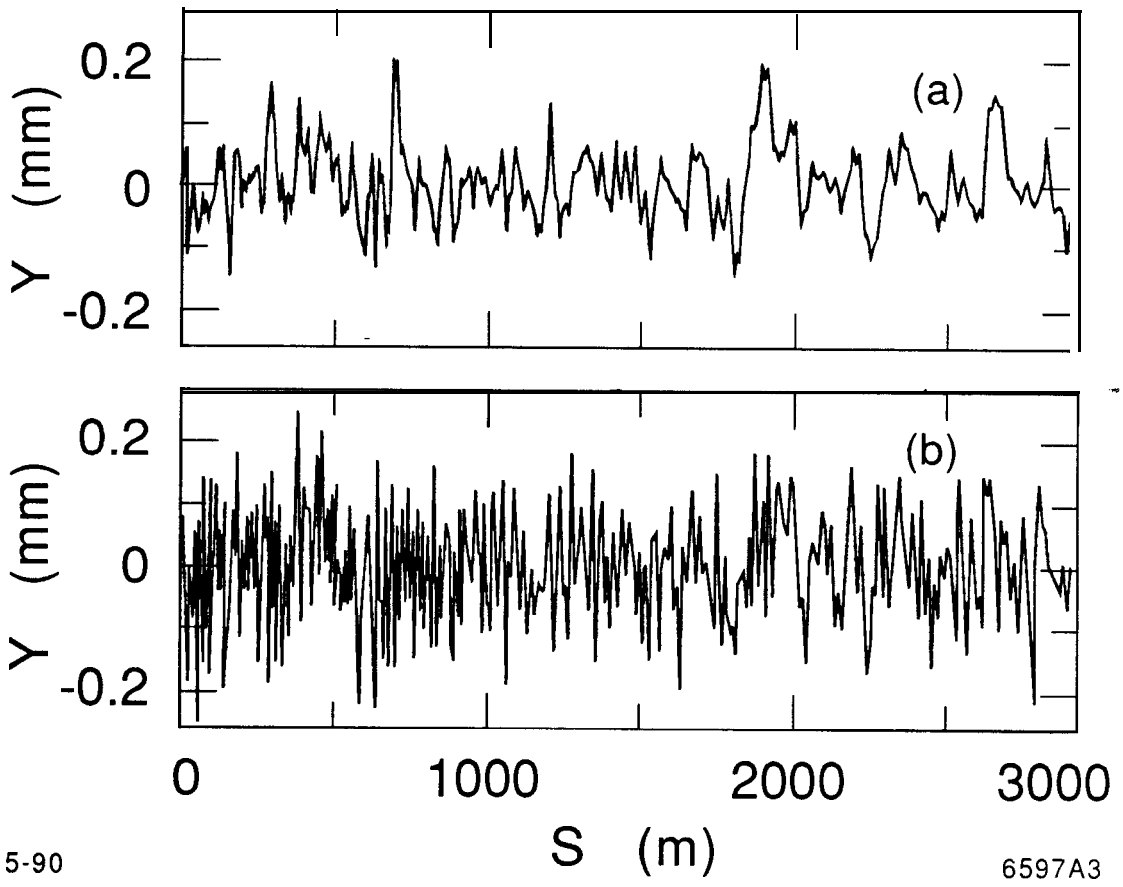

Fig. 3

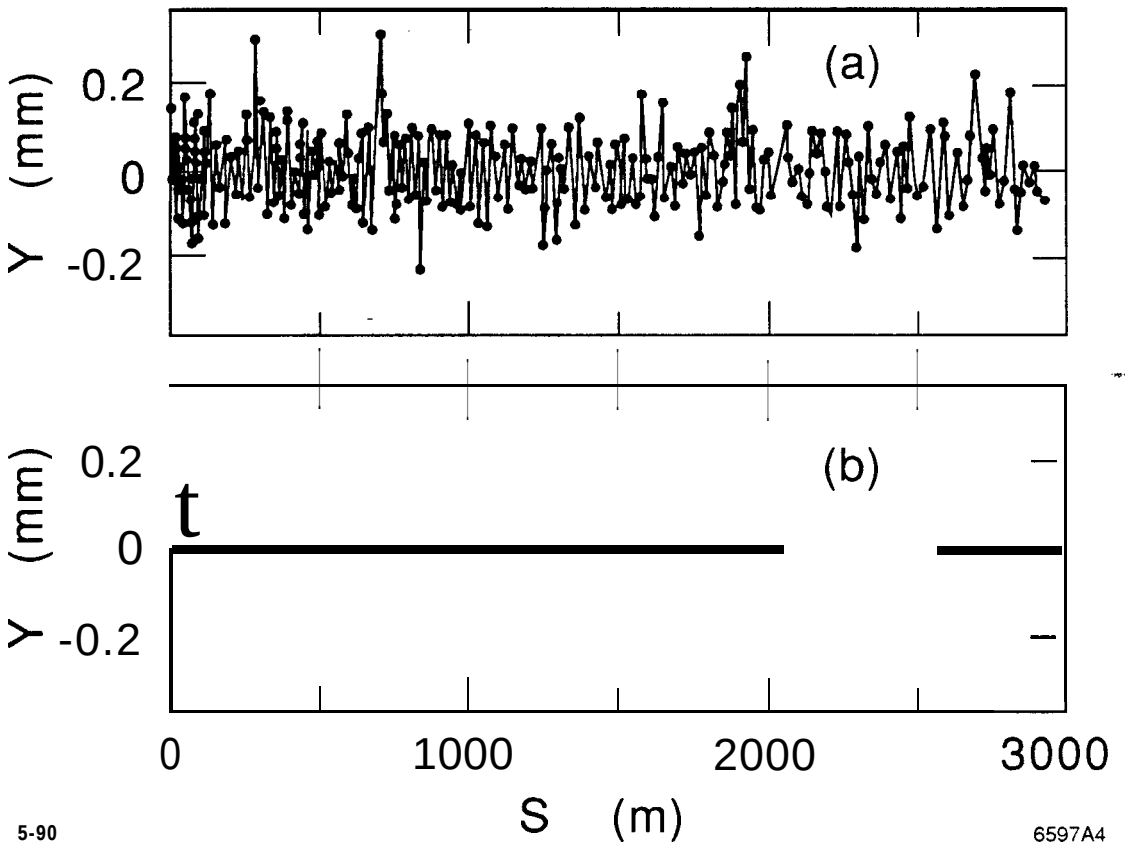

Fig. 4

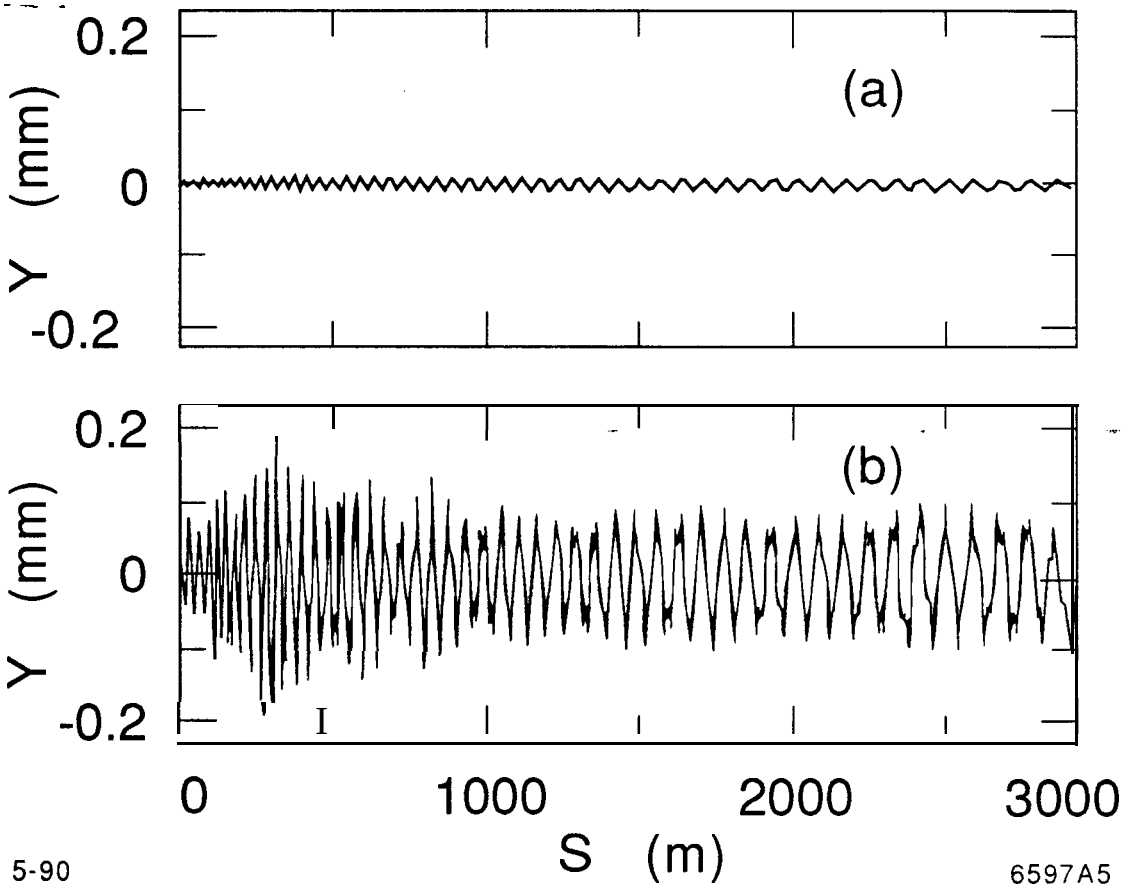

Fig. 5

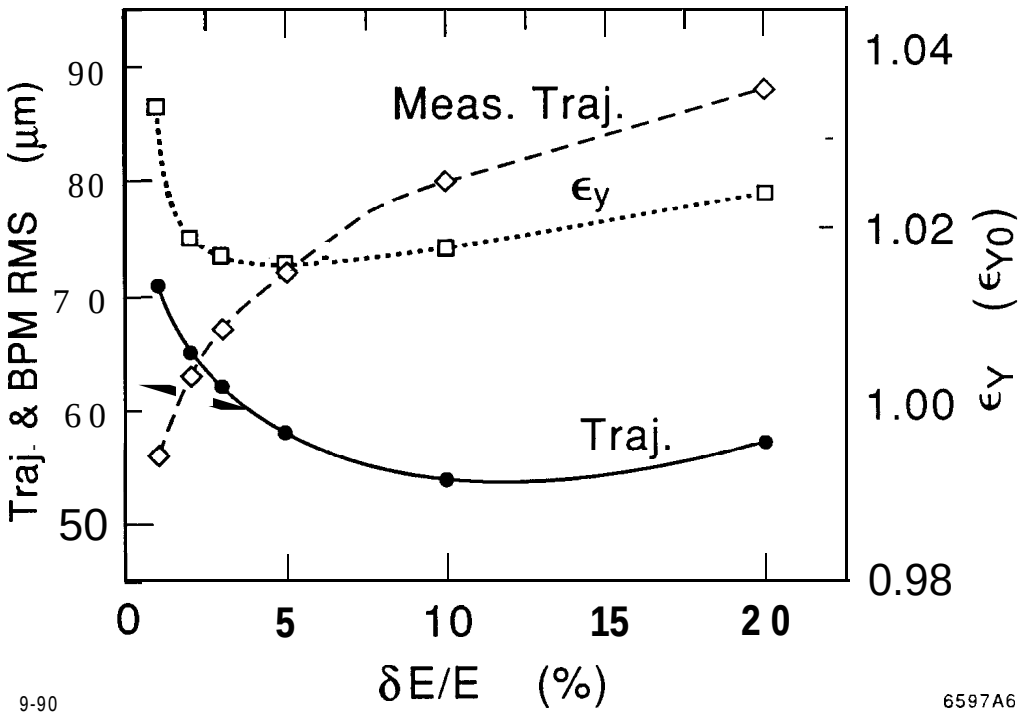
Meas. Traj.
ϵ_y
Traj.
Traj. & BPM RMS (μm)
90
80
70
60
50
0
5
10
15
20
δE/E (%)
1.04
1.02
1.00
0.98
ϵ_Y (ϵ_{Y0})
9-90
6597A6

Fig. 6

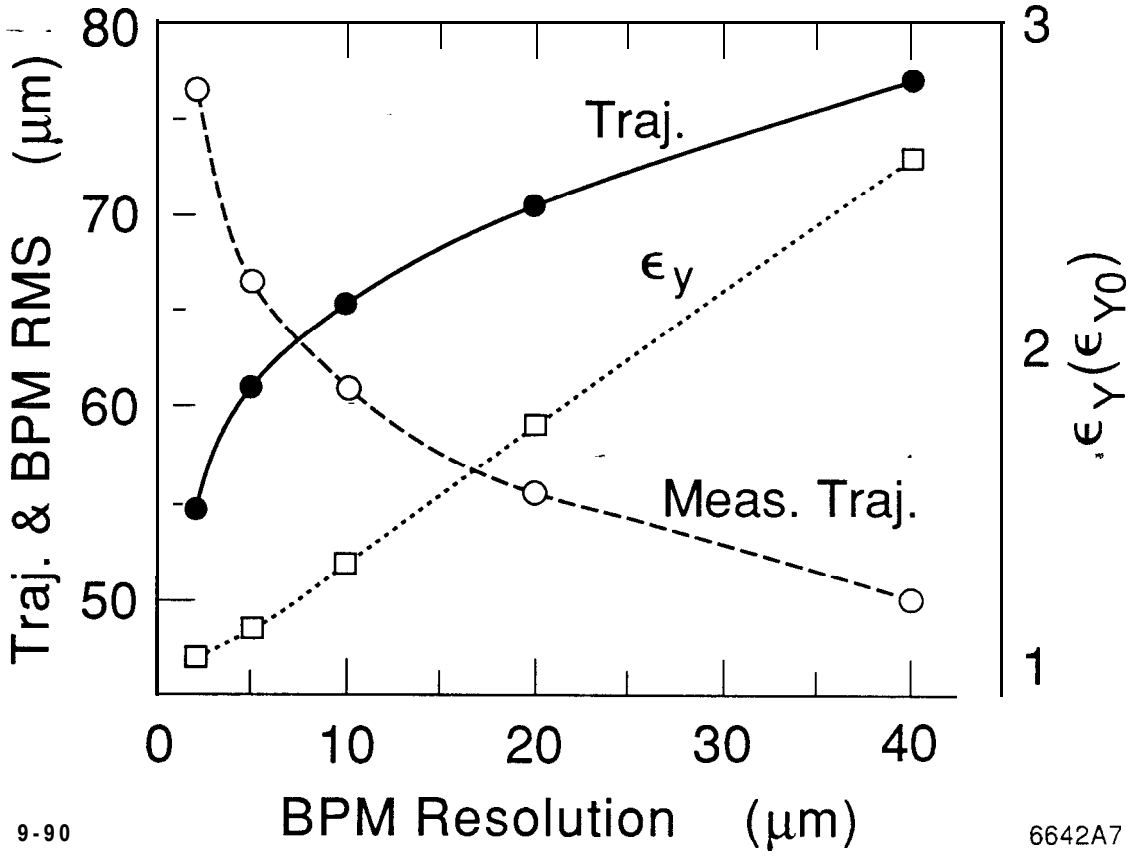
80
70
60
50
Traj. & BPM RMS (μm)
3
2
1
$\epsilon_Y(\epsilon_{Y0})$
Traj.
ϵ_y
Meas. Traj.
0
10
20
30
40
BPM Resolution (μm)
9-90
6642A7

Fig. 7

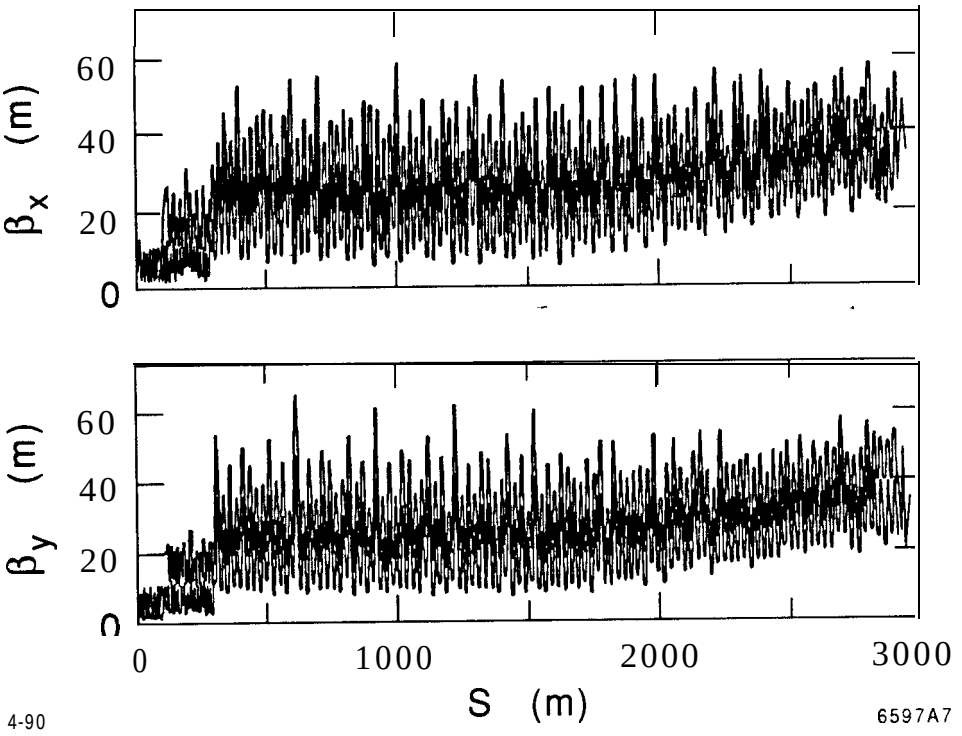
60
40
20
0
β_x (m)
60
40
20
0
β_y (m)
0
1000
2000
3000
S (m)
4-90
6597A7

Fig. 8

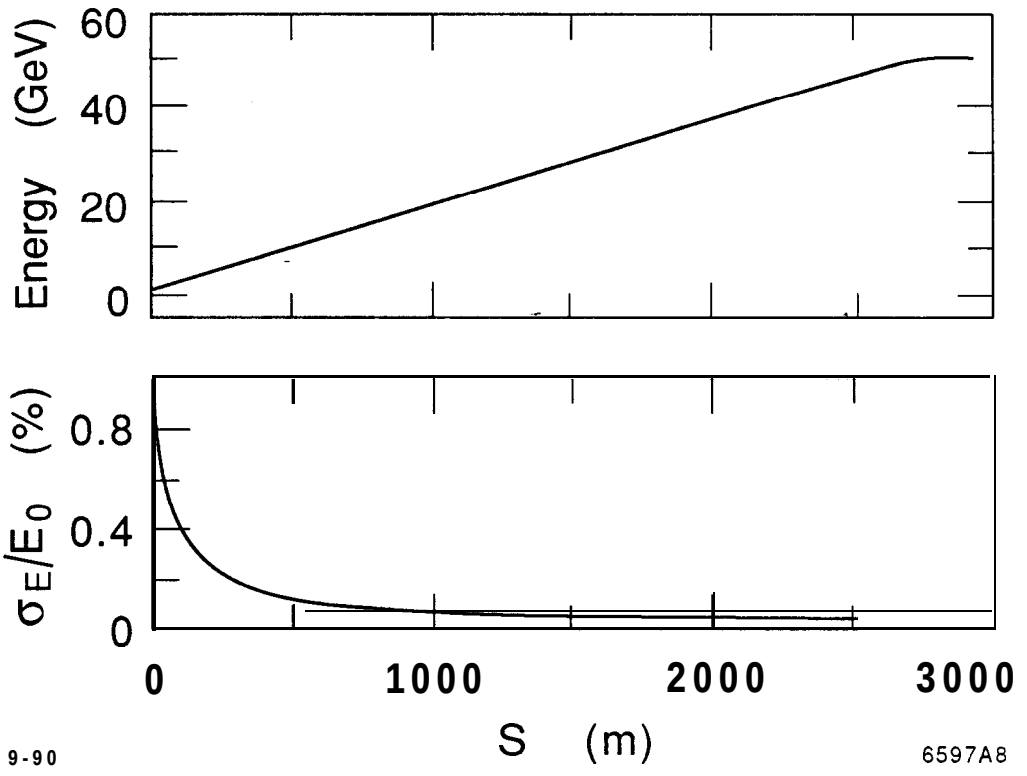
60
40
20
0
Energy (GeV)
0.8
0.4
0
σ_E/E_0 (%)
0
1000
2000
3000
S (m)
9-90
6597A8

Fig. 9

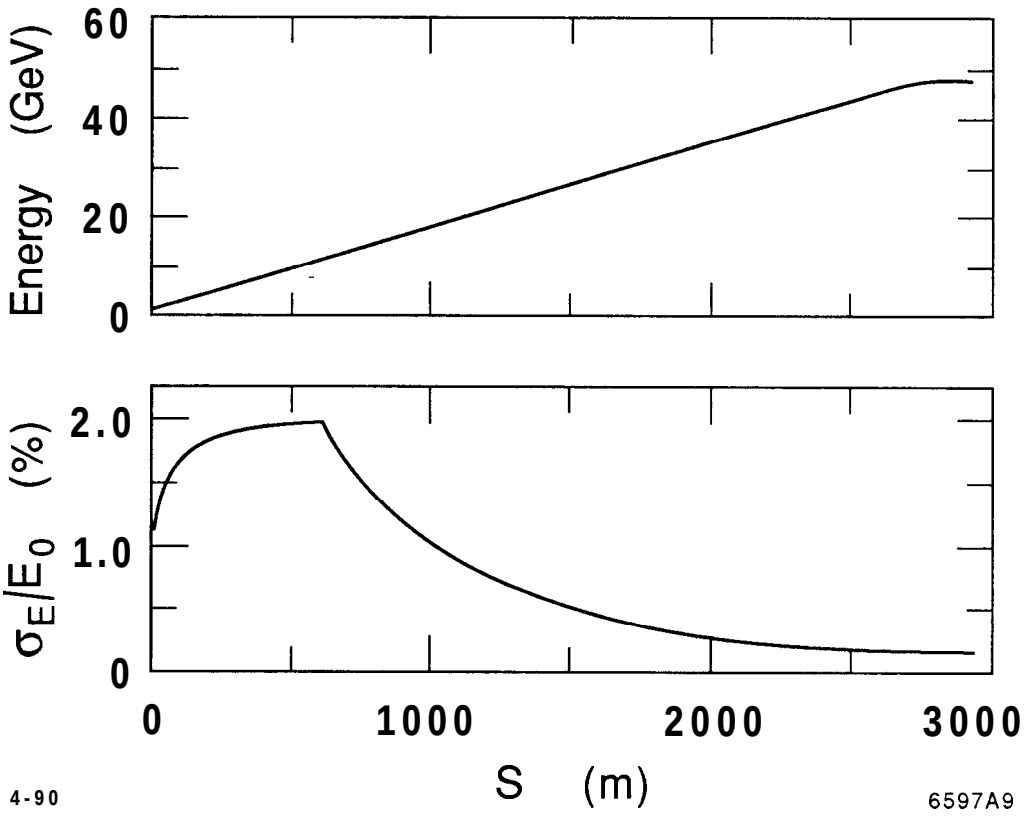
60
40
20
0
Energy (GeV)
2.0
1.0
0
σ_E/E_0 (%)
0
1000
2000
3000
S (m)
4-90
6597A9

Fig. 10

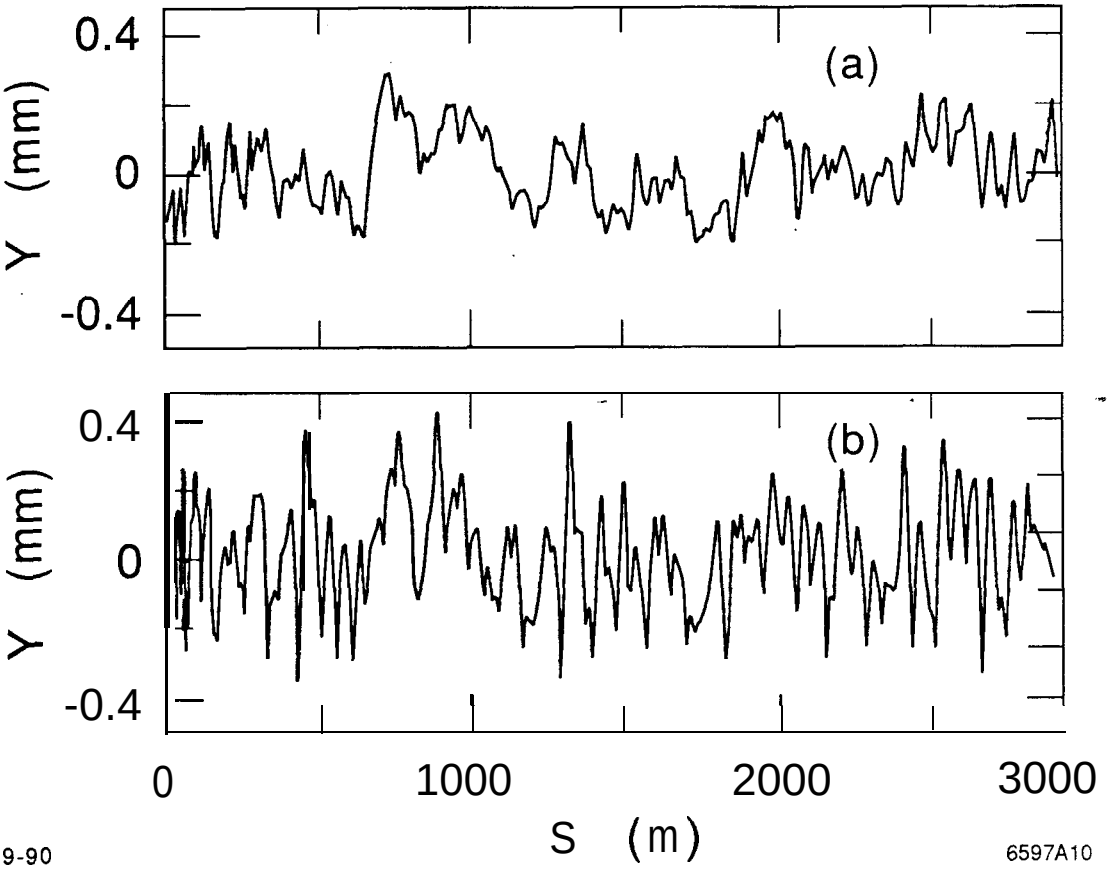

Fig. 11

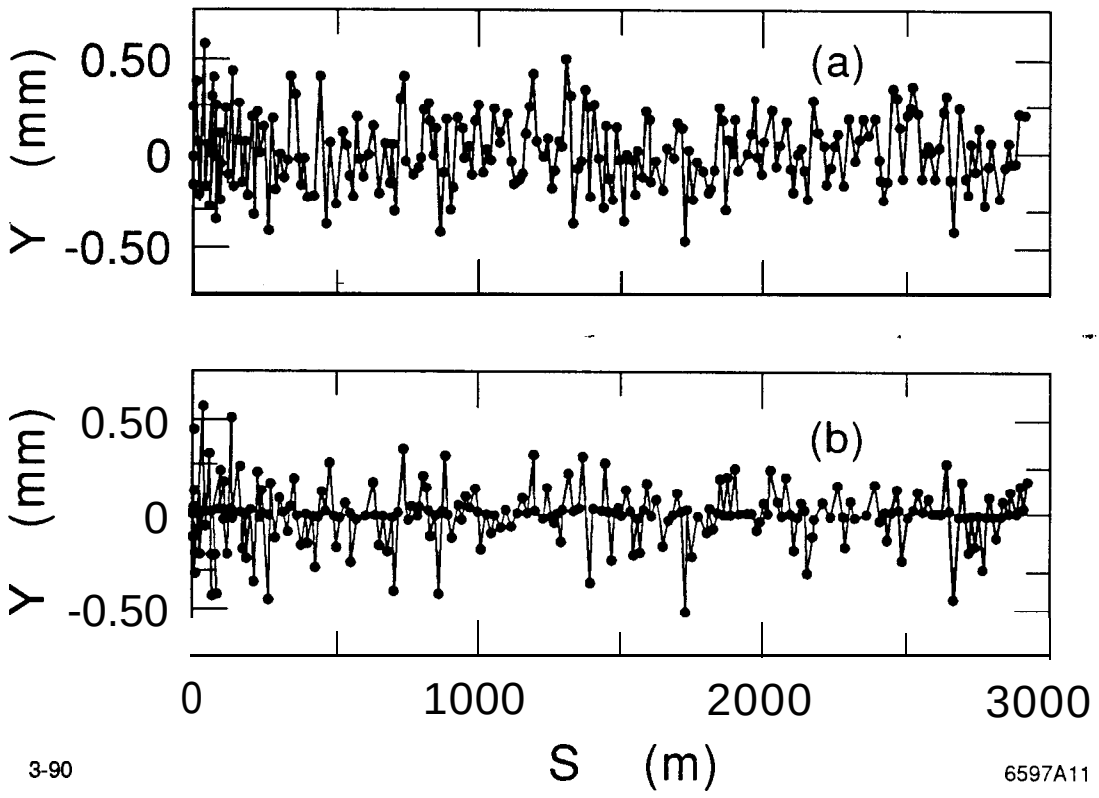

Fig. 12

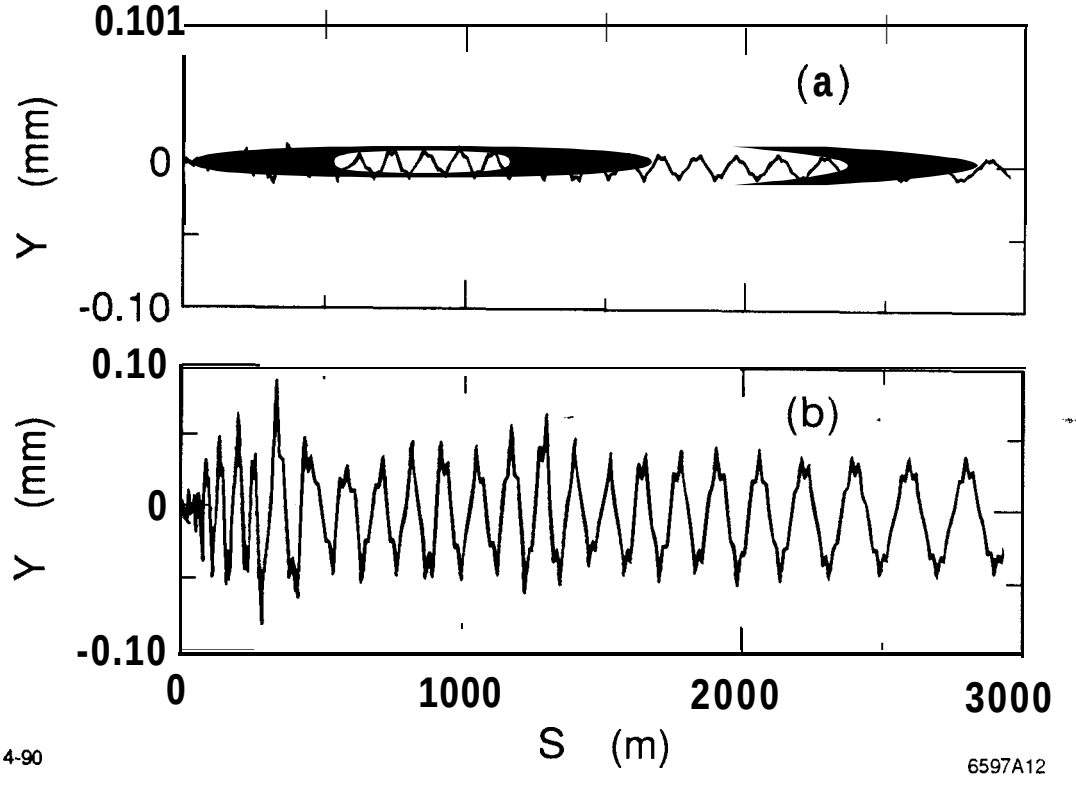

Fig. 13

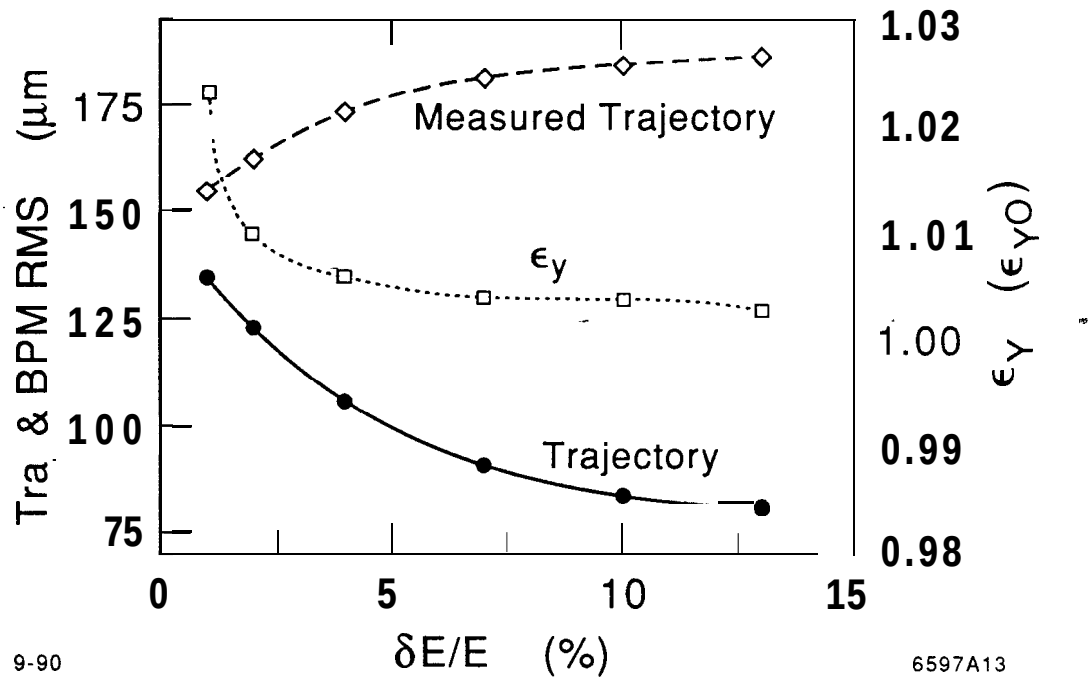
Tra. & BPM RMS (μm
175
150
125
100
75
0
5
10
15
δE/E (%)
1.03
1.02
1.01
1.00
0.99
0.98
εY (εYO)
Measured Trajectory
εy
Trajectory
9-90
6597A13

Fig. 14

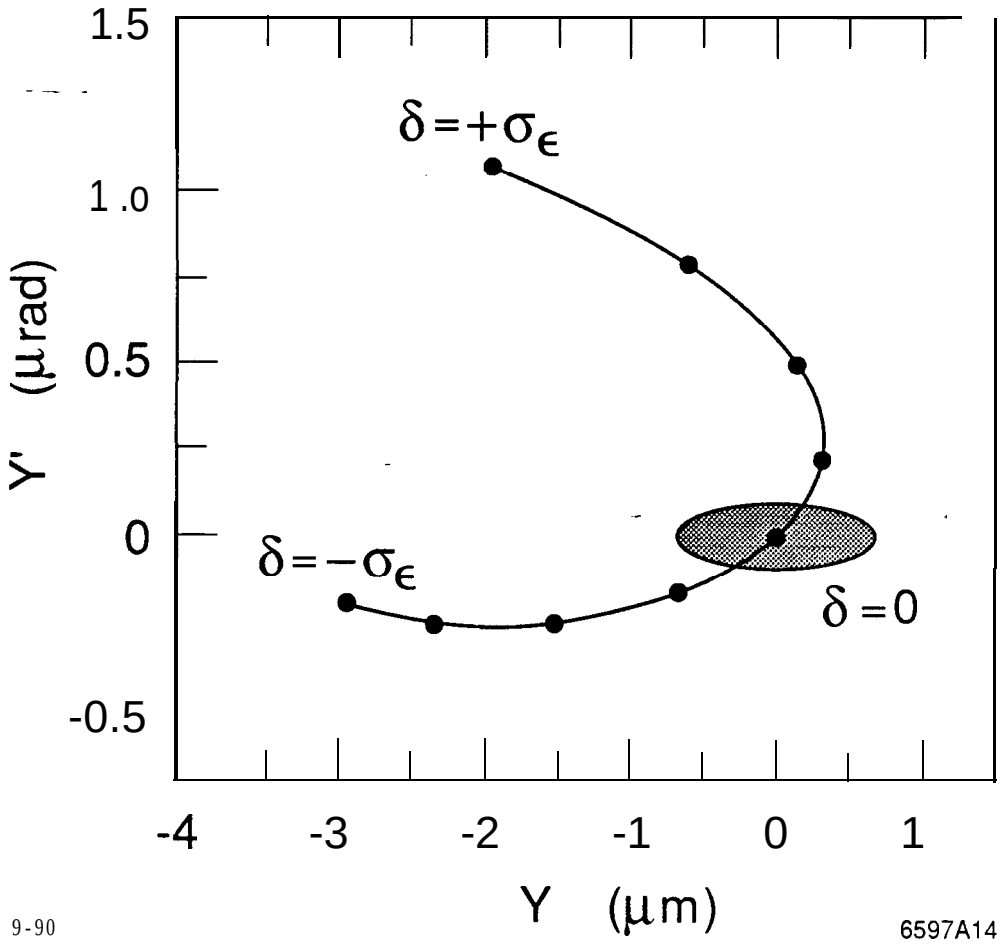

Fig. 15

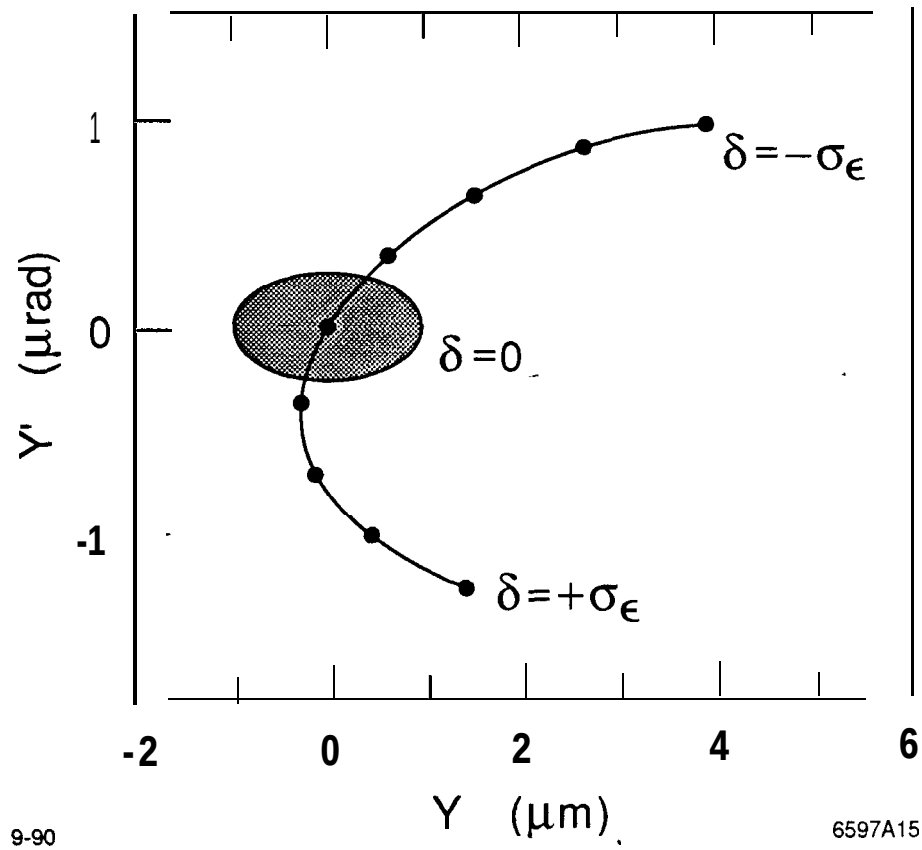

Fig. 16

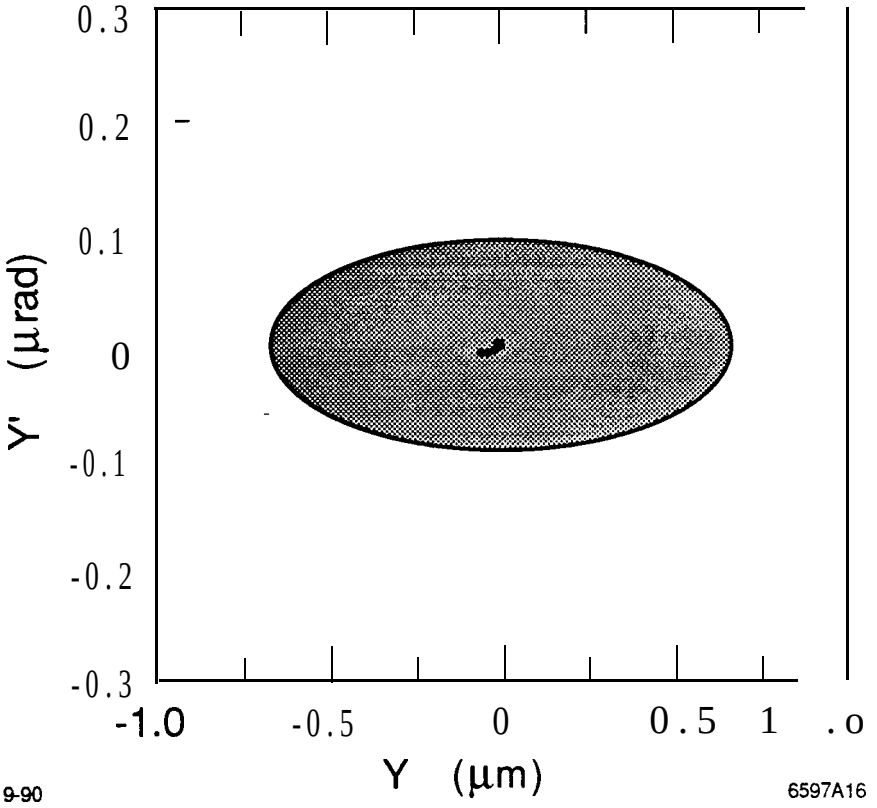

Fig. 17

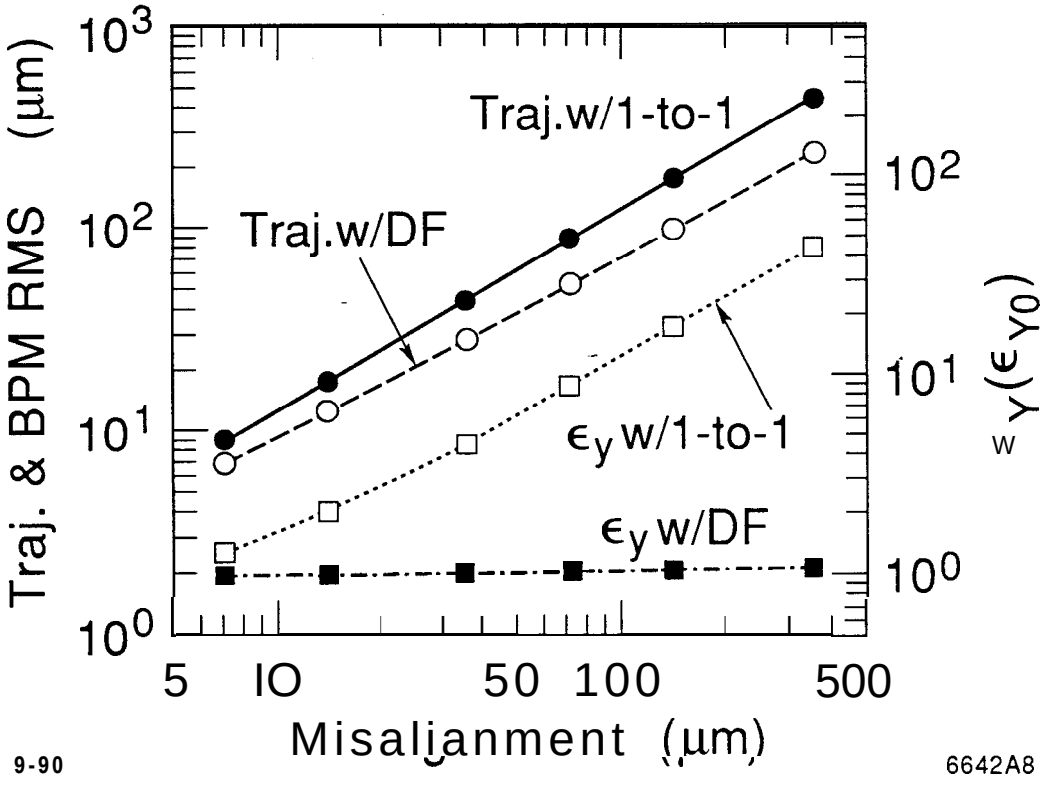
Traj. & BPM RMS (μm)
10^3
10^2
10^1
10^0
Traj.w/1-to-1
Traj.w/DF
ϵ_y w/1-to-1
ϵ_y w/DF
10^2
10^1
10^0
$\epsilon_y(\epsilon_{y0})_w$
5
IO
50
100
500
Misalianment (μm)
9-90
6642A8

Fig. 18